$Cu_{0.5}Tl_{0.5}Ba_2Ca_2(Cu_{3-x}Cs_x)O_{10-\delta}$ (x=0.5,1,1.5,2,2.5,3) Samples and their Superconducting properties

Wajid Ali

Department of Physics

Quaid-I-Azam University

Islamabad, Pakistan

2022

$Cu_{0.5}Tl_{0.5}Ba_2Ca_2(Cu_{3-x}Cs_x)O_{10-\delta}$ (x=0.5,1,1.5,2,2.5,3) Samples and their Superconducting properties

A dissertation submitted to the department of physics, Quaid-i-Azam University, Islamabad, in the partial fulfilment of the requirement for the degree of

Master of Philosophy

In

Physics

By

Wajid Ali

To the

Material Science Laboratory

Department of Physics

Quaid-I-Azam University

Islamabad, Pakistan

2022

In the name of Allah Almighty the most beneficent and merciful, and the most sovereign among all of us.

Certificate

This is certifying that Mr.Wajid Ali S/O Manzar Ali has carried out the experimental work in this dissertation under my supervision in Materials Science Laboratory, Department of Physics, Quaid-i-Azam University, Islamabad and satisfying the dissertation requirement for the degree of Master of Philosophy in Physics.

Supervisor

Prof. Dr. Nawazish Ali Khan
Department of Physics
Quaid-i-Azam University
Islamabad, Pakistan

Submitted through

Chairman

Prof. Dr. kashif Sabeeh
Department of Physics
Quaid-i-Azam University
Islamabad, Pakistan

DEDICATED

TO

MY BELOVED

PARENTS,BROTHERS AND SISTERS AND ESPECIALLY MUNAWAR HUSSAIN(LATE)

Acknowledgment

First and foremost,I would like to praise the Almighty ALLAH, The most beneficent and The most merciful for his blessing given to me during my study and in completing my this research work and thesis. I offer my humble and sincere words of thanks to his Holy Prophet Muhammad (P.B.U.H) who is forever a source of guidance and knowledge for humanity.

I would like to express my gratitude and sincere thanks to my supervisor Prof. Dr. Nawazish Ali Khan for giving me the opportunity to do research and providing invaluable guidance,corrections,comments and suggestions throughout this research so I could complete this thesis on time. His dynamism,vision,sincerity and motivation have deeply inspired me.So once again I am extremely grateful for what he has offered me. My great honor is also bestowed upon all the faculty members of the Physics Department at Quaid-i-Azam University, Islamabad for their invaluable knowledge and assistance they have given to me.

A very special gratitude goes out to my beloved Parents who have been our source of inspiration and who continually provide their moral,spiritual,emotional and financial support.So without their prayers and support the completion of this study task would have been merely a dream for me.

I am also very thankful to my Sisters and Brothers especially I would like to give thanks to Gohar Ali for his love,kindness,motivation and financial support which enabled me to achieve this goal.

I would like to pay lots of appreciation and special thanks to all my Seniors,Lab fellow and friends specially Anila kanwal, Zarmeen Malik, Sadia Firdaus, Ayesha, Ambreen Akhtar, Usama, Zahid Ashiq, Sajid Abbas, Muntazir Hussain, Waseem Nana, Shah Tahir, Rizwan and Jamshid Ali.

Lastly I extended my sincere regards and gratitude to Ali Abbas khan for his constructive suggestions and technical guidance during the whole period of my research work

Wajid Ali

TABLE OF CONTENTS

LIST OF FIGURES

CHAPTER 1

CHAPTER 3

CHAPTER 4

LIST OF TABLES

Abstract

The role of charge carriers suppliers of alkali metal Cs at the CuO2 planes is investigated by preparing $Cu_{0.5}Tl_{0.5}Ba_2Ca_2(Cu_{3-x}Cs_x)O_{10-\delta}$ (x=0.5,1,1.5,2,2.5, 3) superconductor samples. These samples have shown orthorhombic crystal structure in which volume of the unit cell suppresses with the increased Cs-doping. A metallic variation of resistivity is a typical feature of these samples in which an enhancement is observed in the critical temperature with increased Cs-doping. The excess conductivity analyses of conductivity data have shown enhancement in coherence length along c-axis $\xi_{c(0)}$, the inter-layer coupling J and Fermi velocity V_F of superconducting carriers and the phase relaxation time τ_φ of the superconducting carriers with increased Cs-doping. In comparison with un-doped $Cu_{0.5}Tl_{0.5}Ba_2Ca_2Cu_3O_{10-\delta}$ samples the values of parameters such as $B_{c(0)}$, $B_{c1(0)}$, $B_{c2(0)}$, $J_c(0)$ and $\kappa=\lambda/\xi$ are suppressed in Cs-doped $Cu_{0.5}Tl_{0.5}Ba_2Ca_2(Cu_{3-x}Cs_x)O_{10-\delta}$ (x =0.5, 1, 1.5, 2, 2.5, 3) samples showing suppression in the population of inadvetent defects which act as pinning centers. Oxygen related phonon modes are softened in Cs-doped samples demonstrating intrinsic doping of Cs in the final compound. Dielectric measurements of these samples have shown suppression in the values of the real part of dielectric constant ε', imaginary of part of the dielectric constant ε'' and ac-conductivity σ_{ac} that most likely arises from the the suppression in the density of holes due to increased electron-holes recombinations that transform the material to optimal doping regime which result to their higher critical temperature.

CHAPTER-01
1 INTRODUCTION TO SUPERCONDUCTIVITY

This chapter discusses the emergence of the phenomenon of superconductivity, its brief historical evolution and different theories that gives insight understanding of the given phenomenon. In the end, the chapter consists of some applications of superconductivity.

1.1 Superconductivity and its historical evolution

A Superconductivity is a phenomenon in which specific materials, known as superconductors, exhibit completely zero electrical resistance and magnetic field exclusion when cooled below a characteristic critical temperature Tc. [1]. So we know that the critical temperature is the transition temperature of a material among its superconducting and its normal state.

The history began in 1911 when a Dutch physicist H. Kamerling Onnes discover superconductivity in mercury. Below 4.2 kelvin(k)[2] he found that resistance abruptly drops to and in next year he discovered that, resistance is restored by the application of the strong magnetic field.

Superconductors have perfect diamagnetism, as discovered in 1933 by W. Meissner and R. Ochsenfeld. [3]. The Meissner effect, which was discovered, is the exclusion of magnetic fields from the interior of materials that have cooled below their transition temperature at the presence of a weak magnetic field.

C. J. Goater and H. B. G. Casimir proposed the two-fluid model in 1934, based on the assumption that there are two components of conducting electron fluid in the superconducting state,one of which is the normal electrons originating from normal metals and the second is superconducting electrons attribute to anomalous properties that leads to the phenomenon of superconductivity [4].

The presence of the two critical magnetic fields in type II superconductors was proven in 1937 by L. V. Shubnikov et al. [5].So the existence of a two critical magnetic field attribute to vortices and this new state is called "mixed state" or "Shubnikov's phase". A. A. Abrikosov theoretically explained Shubnikov's experiment with the help of a Ginzburg-Landau

theory proposed by V. Ginzburg and L. Landau in 1940 [6-7]. He suggested that vortices found in Shubnikov's phase formed periodic lattice.

In 1950, H, Frolich proposed that vibrating atoms play a key role in making materials a superconductors. Based on his assumption, E. Maxwell and C. A. Reynolds discovered the isotope effect of mercury and calculated the critical temperature and isotope mass "M"

[8-9] i.e.

$$T_c M^{1/2} = \text{constant} \qquad (1.1)$$

In 1957, J. Bardeen, L. Cooper, and R. Schrieffer proposed the microscopic theory of superconductivity in metals known as BCS theory [10]. According to the BCS theory,the superconductivity is caused by weak electron-phonon interactions, where two electrons that join to create a Cooper pair exhibit an attractive potential.

The Josephson effect, which is the quantum-mechanical tunnelling of Cooper pairs over a small insulating barrier placed between two a superconductors was first theorised by B. D. Josephson in 1962.

In 1984 a bi-soliton model was put up by L. S. Brizhik and A. S. Davydov to account for superconductivity in organic quasi-one-dimensional conductors[11]. A cooper pair in this model is a quasi-one-dimensional excitation due to the coupling of the strong, nonlinear, electron-phonon interactions.

P. Anderson proposed a model in 1987 to explain the mechanism of a superconductivity in a cuprates, postulating that a pairing mechanism and the establishment of phase coherence are different mechanisms from each other. [12].

In 1990, A. S. Davydov published a theoretical model describing how superconductivity works in superconductor having a high 'T_c' especially cuprates [13]. The central idea of his theory is to use the concept of bi-solitons.in this concept,electrons are attracted to each other by a local deformation of the CuO_2 planes' -O-Cu-O-Cu- chain.

In 1995, V. J. Emery et al. consider the pairing mechanism and a long range phase coherence to be a fundamental mechanisms of well-established superconductivity. They emphasized above 'T_c' cooper pairs begin to form and that at T_c (R=0) the long-range phase

coherence is strong[14].

In 1999, it is found from tunnelling and neutron scattering measurements that the magnetic resonance peak appearance is due to the spin excitation that causes phase coherence in $Bi_2Sr_2CaCu_2O_{8+x}$ (Bi-2212) and $YBa_2Cu_3O_{6+x}$ (YBCO). [15].

In the previous decades after the discovery of unconventional superconductors, specially cuprates, many theories presented by different scientists to understand the mechanism of superconductivity, but unfortunately, there is no proper and complete theory fully explaining the given mechanism, and it is an open debate for the physicists in the field of condensed matter to formulate the complete theory of superconductors.

1.1.1 Era of High Temperature Superconductors

In the early years following the discovery of mercury's superconductivity, numerous elemental metals like lead (T_c = 7.2K) and niobium (T_c = 9.2K) show superconductivity, the later has highest critical temperature in elemental metal [16]. Many new superconductors were discovered between 1964 and 1986 and all obey BCS theory, which imposed an upper limit to T_c of about 30K under strong coupling limit [17]. The era of high temperature superconductors began after superconductivity was discovered, in one of cuprates family La-Ba-Cu-O having a maximum T_c of about 38K [18]. In 1987, the transition temperature of 93K was discovered in YBCO [23]. In the next year, Bi and Tl based superconductors having T_c 110K and 125K were discovered respectively.

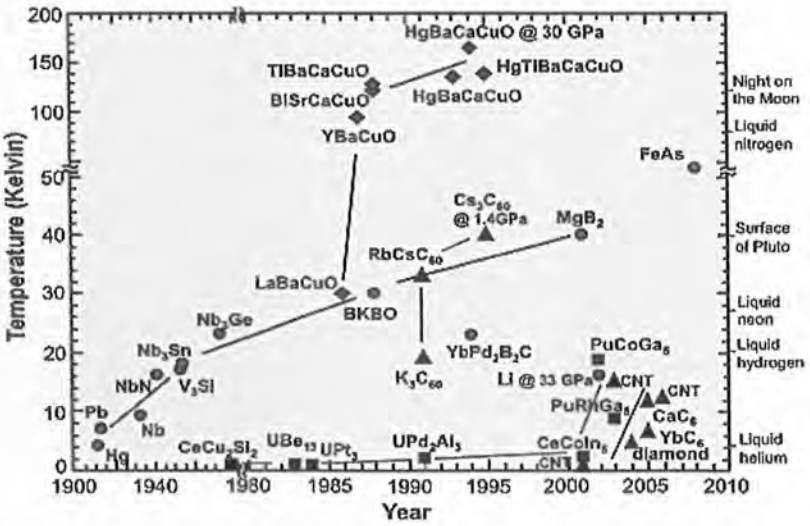

Figure 1-1:The Critical Temperature of a Different Materials along with years.

In 1993 Hg based superconductors discovered with the highest T_c of about 135K that extend to 164K by applying pressure [19]. In 2015, Eremets et al. discovered that sulphur hydride shows T_c of about 203K under pressure of 90 gigapascals [26]. Recently in 2018, R. Hemley et al. discovered superconductivity in lanthanum hydride LaH_{10} having T_c 280K by applying pressure of 200 gigapascals. The superconductor material discovered by Eremets and Hemley under high pressure are conventional superconductors and these types of superconducting materials have been well understood since 1950s.

1.2 Properties of superconducting state

In the following section, we will discuss some anomalous properties of the superconducting state.

1.2.1 Zero resistivity

The zero resistivity is one of the most prominent characteristics shown by superconductors. One can observe a sudden change in resistivity from finite value to zero at critical temperature T_c (R=0),as given in figure 1-2.

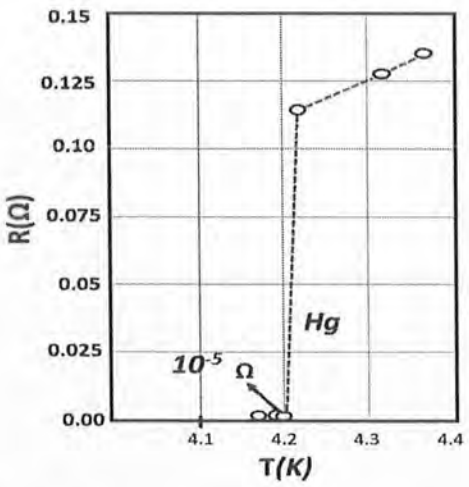

Figure 1-2:The Resistivity vs Temperature Graph of a Mercury.

The above figure shows the certain change in resistance around 4.2 K for mercury which point out the occurrence of thermodynamic phase transition from one phase to another [20]. One of the phases, occurred at temperature value higher than 4.2 K, referred to as normal phase in

which superconducting material behave like normal metal and their properties like electrical and magnetic show the same behaviour as that of metal at ambient conditions. While the other exist at temperature value lower than 4.2 K is a superconducting phase in which electrical and magnetic properties are quite different i.e. zero resistivity and perfect diamagnetism.

1.2.2 A Meissner-Ochsenfeld effect

The Meissner-Ochsenfeld effect refers to the exclusion of a magnetic field from the interior of a superconductor upon cooling to its critical temperature and was first investigated by Meissner and Ochsenfeld[21]. This effect occurs when the magnetic field (B) is applied to a superconducting material placed below 'T_c' and penetrates through a small thickness λ. A current builds up on its surface, cancelling the effects of an external magnetic fields and creating magnetization inside the superconducting material. Superconductors in the Meissner state exhibiting perfect diamagnetism with negative values of susceptibility "χ",i.e.

$$\chi = -\mu_0 M/B = -1 \qquad (1.2)$$

so here 'μ_0' is a permeability for a free space and 'M' for the magnetization.

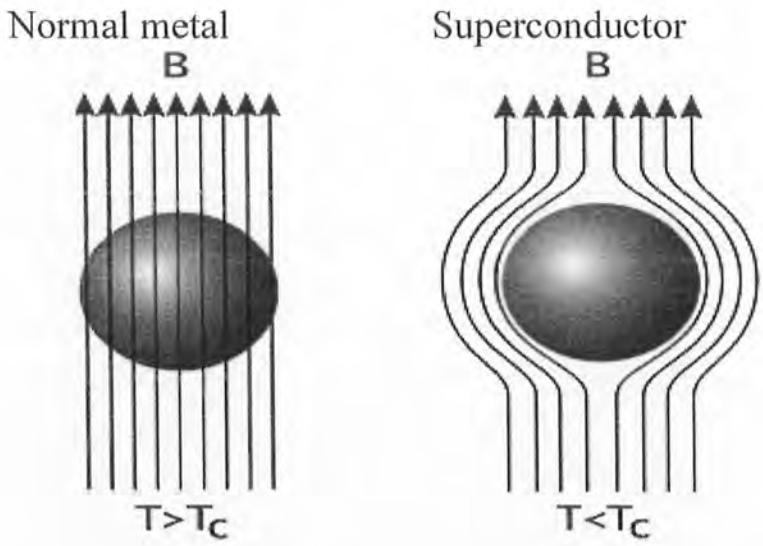

Figure 1-3:Meissner Effect

If we put a superconductor in a magnetic field at $T > T_c$, and further decrease the temperature to reach that the $T < T_c$, then the magnetic field in this case is confined within the superconductor and will diminish if we increase the temperature through T_c. So this "frozen"

magnetic field is independent of a external magnetic field(b) when removed and remains inside the superconductor.

1.2.3 A Flux quantization

A Quantization of a magnetic flux is a quantum property of a superconducting state. When $T<T_c$, the magnetic field lines will trap in nonsuperconducting holes(voids) as shown in figure 1.4. The magnetic field lines generated by supercurrents on the inner surface of the hole. The equation for flux quantization is

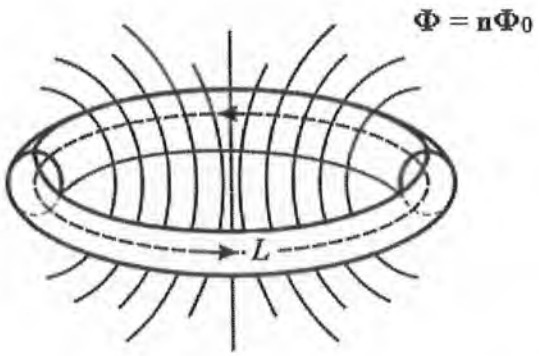

Figure 1-4:Quantization of Magnetic Flux

$$\Phi = \frac{2ne}{e^*}\Phi_0 \qquad n = 1, 2, 3, 4..... \qquad (1.3)$$

Where Φ_0 is flux quantum having value $\frac{hc}{2e} = 2.0679$ G cm^2 and Φ is total flux stored in a hole. The equation 1.3 manifest that flux through hole in a superconductor is quantized in unit of $\frac{2e}{e^*}\Phi_0$. Here e^*=2e, reflected the fact that pairing of electron leads to the occurrence of superconductivity.

1.2.4 A Josephson effects

B. D. Josephson proposed a theoretical explanation for quantum-mechanical tunnelling of Cooper pairs via a thin insulating barrier sandwiched between two superconductors in 1962. That theoretical explanation was soon experimentally verified and is named as the Josephson effect. In a Josephson effect ,electrons from two superconductors fuse into a single quantum body. The wavefunction of electrons on either side of the insulating layer interact via a weak link. Consequently, the same wavefunction describe all the electron on both sides of a weak link. Due

to a weak link or inhomogeneity, a phase difference of $\theta = \theta_1 - \theta_2$ created between two superconductors.

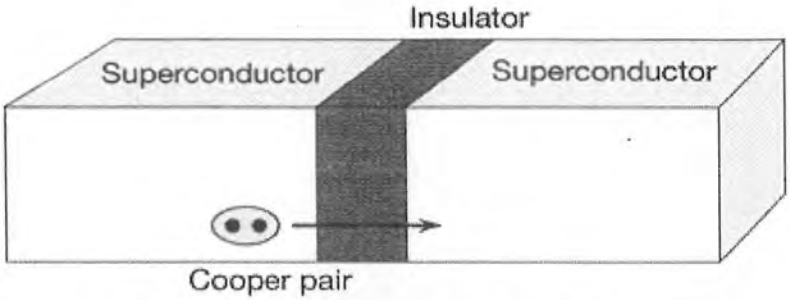

Figure 1-5:Schematic Diagram of SIS Tunnelling Junction

So we have two types of Josephson effects in which one is DC Josephson effect and the second one is AC Josephson effect. In DC Josephson effect, a direct current flows through a weak link when no external voltage is applied. The basic equation that describes this effect is

$$I = I_c sin\theta \qquad (1.4)$$

where I is a current and I_c is a critical current through a Josephson junction. DC values are between $-I_c$ and I_c. In AC Josephson effect, applying a voltage (V) across a junction causes a phase change with time which is given by the equation.

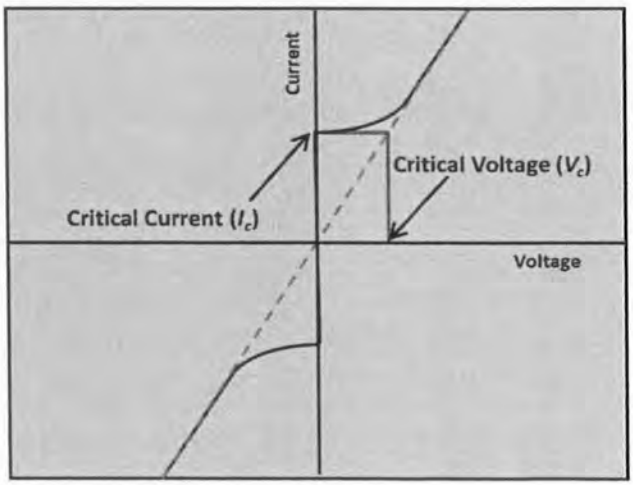

Figure 1-6:I-V Characteristic of SIS Tunnelling Junction

$$\frac{\partial\theta}{\partial t} = \frac{2e}{\hbar}V \qquad (1.5)$$

The phase changes linearly with time and alternating current generated having amplitude I_c. So that the complete mathematical equation for I_{ext} (alternating current) is

$$I_{ext} = C_j \frac{dv}{dt} + I_c \sin\theta + \frac{V}{R} \qquad (1.6)$$

Where C_j is a constant

1.3 Basic theories of superconductivity

1.3.1 The London theory

In 1935, two brothers named Fritz and Heinz London presented the first phenomenological theory of superconductivity. They describe two fluid models, which state that there are two components of a conducting electron fluid in the superconducting state,one fluid component consisting of normal electrons having density n_n,which behaves similarly to the free electrons of normal metals. The second component of fluid consist of superconducting electron that leads to the cause of superconductivity.To formulate the two equations, they assume that the superconducting electron density n_s is same everywhere i.e. there is no spatial variation in n_s. The also hypothesized that electric and magnetic fields are so weak that they have no effect on charge carriers.

There are two London equation formulated by London brothers. The first London equation describes the dynamics of superfluids in the presence of an electric field and builds a relationship between changes in the superconducting charge density j_s in response to an electric field i.e.

$$\frac{dj_s}{dt} = \frac{n_s e^2}{m}E \qquad (1.7)$$

The second London equation describes the response of superconducting materials at a presence of applied magnetic field (B) which successfully explains the Meissner effect. Mathematically it is represented as:

$$\vec{\nabla} \times \vec{J_s} = \frac{n_s e^2}{m}\vec{B} \qquad (1.8)$$

$$j_s = \frac{cH_0}{4\pi\lambda} e^{\frac{-x}{\lambda}} \qquad (1.9)$$

The above equation shows that the magnetic field does penetrates to a shallow depth on the surface of the material with a penetration depth of λ.

1.3.2 London Penetration depth

It is the characteristic length that defines how far 'B' penetrates the superconductor. The magnetic field is not cancelled completely but is exponentially screened from the inside of superconducting material. Values of vary λ_L between 50 and 500nm.

$$\lambda_L = (mc^2/4\pi n_s e^2)^{1/2} \qquad (1.10)$$

It obeys that screening super current at superconducting surface shows decrement over same length.

$$B = B_o e^{-x/\lambda L} \qquad (1.11)$$

$$Js = (c/4\pi)\ curlB \qquad (1.12)$$

So we get Js for our simpler geometry as

$$Js = (cB_o/4\pi\lambda_L)e^{-x/\lambda L} \qquad (1.13)$$

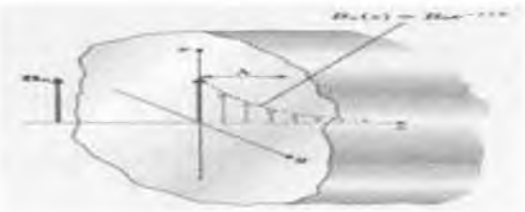

Figure 1-7:A Exponential Decay of a Magnetic field inside the Superconductor.

From (1.10) we can see that λ_L is temperature dependent because it depends on n_s. So

$$\lambda(T)=\lambda(0)/\sqrt{[1-(\frac{T}{Tc})\text{^}1/4]} \qquad (1.14)$$

1.3.3 The Ginzburg-Landau (GL) theory

V. L. Ginzburg and L. D. Landau published the first quantum theory of superconductivity in 1950[22]. The quantum effects were not taken into account by the London theory. However, a need for quantum theory was strongly felt because firstly, the superconducting state's entropy is lower than the normal state's,and secondly, a transition from normal state to superconducting state is a second-order phase transition that led to idea of an order parameter Ψ.In superconducting electron the order parameter is the complex wavefunction which is zero for $T>T_c$ and non-zero for a $T<T_c$. The Landau theory of the second order phase transition, which is based on the free energy expansion with respect to the small power order parameter Ψ at the transition temperature, was applied in the GL theory.

Therefore, this theory is valid near the critical temperature, i.e. $T-T_c \ll T_c$. Regarding the formulation of the theory, they used normalized version of order parameter which is $|\Psi|^2$ that gives the density of superconducting electron i.e.

$$|\Psi|^2 = {}^{n_s}/_{2} \qquad (1.15)$$

Where 'n_s' is density of electrons of a superconductor.

Further they assumed that a Ψ doesn't depends upon the position r, which means that there is no external field applied that make Ψ a position dependent. Mathematically the expansion of free energy is

$$F = F_n + \alpha|\Psi|^2 + \frac{\beta}{2}|\Psi|^4 \qquad (1.16)$$

Here, F is the free energy density, $F\,n$ is the free energy density in normal state, and 'α' and 'β' are the phenomenological expansion coefficients that are dependent on the superconducting material.The application of a magnetic field (B) will cause the expansion of free energy to become.

$$F = F_n + \alpha|\Psi|^2 + \frac{\beta}{2}|\Psi|^4 + \frac{1}{2m^*}|(-i\hbar\nabla - 2e^*A)\Psi|^2 + \frac{|B|^2}{2\mu_0} \qquad (1.17)$$

Here A is the vector potential.

After minimizing the above equation, we get two generalized equation of GL theory i.e.

$$\alpha\Psi + \beta|\Psi|^2\Psi + \frac{1}{2m^*}\left(-i\hbar\nabla - \frac{e^*}{c}A\right)^2\Psi = 0 \qquad (1.18)$$

$$j_s = -\frac{i\hbar e}{2m^*}(\Psi^*\nabla\Psi - \Psi\nabla\Psi^*) - \frac{2e^2}{mc}|\Psi|^2 A \qquad (1.19)$$

Coherence length ξ and penetration depth λ are two characteristic lengths of a Ginzburg-Landau theory and are given below.

$$\xi = \sqrt{\frac{\hbar^2}{2m|\alpha|}} \qquad (1.20)$$

$$\lambda = \sqrt{\frac{m}{4e^2\Psi\mu_0}} \qquad (1.21)$$

The coherence length represents the length of order parameter or thermal fluctuation and λ represents the penetration depth of magnetic field(B) at a surface of superconducting material. Based on these two parameters Ginzburg-Landau introduce an additional parameter "κ" known as GL parameter define as

$$\kappa = \frac{\xi}{\lambda} \qquad (1.22)$$

where

|Ψ(r)| 2=1 in superconducting state and |Ψ(r)| 2=0 in normal state.

The two length dependent parameters of superconductor are:

- ❖ Coherence length
- ❖ Penetration depth

1.3.4 Coherence Length (ξ)

"ξ" is the length in which order parameter "Ψ" changes nearby the superconducting boundary. This idea was given by Pippard in 1953. The penetration depth and coherence length both are temperature dependent and their ratio is called GL parameter "κ", which differentiates the a Type I and a Type II superconductors [22].

when $\kappa << \sqrt{1/2}$ then it is a Type I Superconductors.

when $\kappa >> \sqrt{1/2}$ then it is a Type II Superconductors.

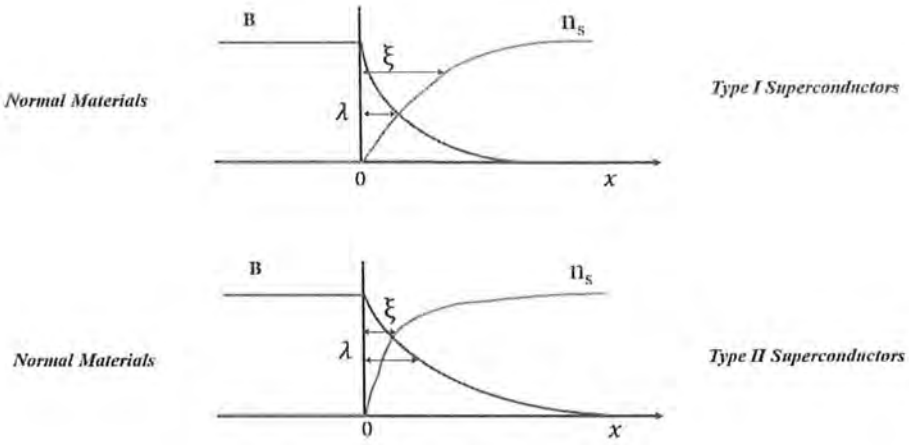

Figure 1-8:Types of a superconductors which is based on penetration Depth and Coherence Length.

1.3.5 Types of a Superconductors

The Superconductors are divided in a Type I superconductor and a Type II Superconductor with respect to their magnetic properties. A Type I Superconductor include all superconductors other than Niobium where Type II superconductors are composed of High 'T_c' superconductors, superconducting alloys, Niobium, and the chemical compounds[11]. while studying the superconducting alloys in a strong magnetic fields the L. Shubnikov experimentally observed the Type II superconductors. According to V. Ginzburg and L. Landau, those with the positive free energy of the normal metallic superconducting interface are Type I superconductors, and those with inhomogeneous states in a strong external magnetic field are Type II superconductors. But at that time only Type I superconductors were known. The theory for Type II superconductors was further refined by A.A. Abrikosov[23].

1.3.5.1 Type-I superconductors

The Superconductors that exhibit a change from a diamagnetic to a paramagnetic state at critical values of applied magnetic field are called Type I Superconductors.Such superconductors strictly obey Meissner effect i.e. below critical field they are perfectly diamagnetic but their magnetization goes to zero for all fields above critical field. They are also called as soft

superconductors because require very small critical field to destroy superconductivity. Pb, Hg, Sn are Type-1 superconductors which perfectly obey the diamagnetic behavior[24].

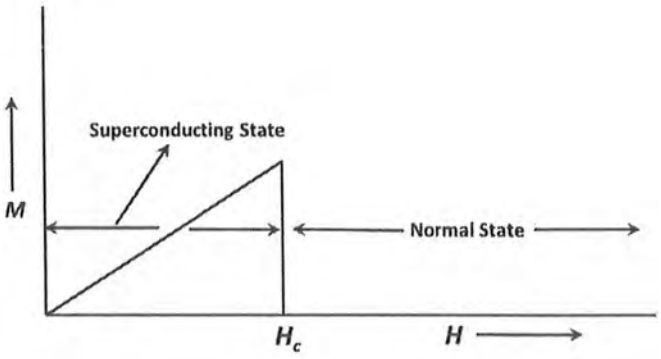

Figure 1-9:Magnetization vs Applied Field of Type-1 Superconductor

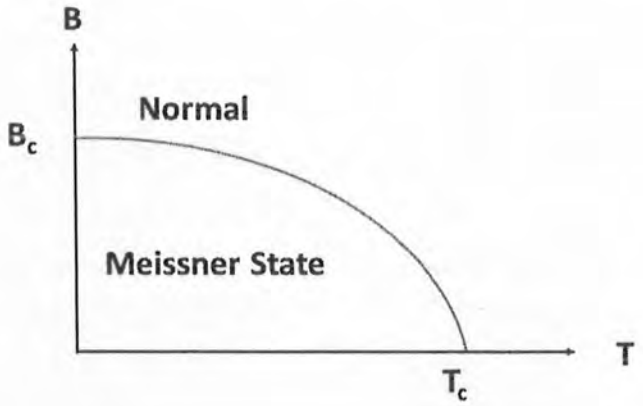

Figure 1-10:Phase illustration of Type-1 Superconductor

1.3.5.2 A Type-II Superconductors

These superconductors do not exhibit such a change from diamagnetic to paramagnetic state and also do not obey the Meissner effect. The magnetic flux penetrates through the specimen at a critical magnetic field 'Hc1' which is called lower critical field and the specimen is in

superconducting state below it. This lower field is less than Hc. The specimen is in normal state (paramagnetic) above Hc2 which is known as upper critical field (100 times greater than Hc). Between Hc1and Hc2 the specimen exhibits mixed state. Magnetic field infiltrates in mixed state in form of vortex and supercurrent circulates around the central core of every vortex. The field penetrating through the vortex tends to oppose the filed from the specimen outside the vortex. These superconductors are also called as hard superconductors as strong magnetic field is needed to finish superconductivity. Ni and metal alloys are samples of type-II superconductors. [25]

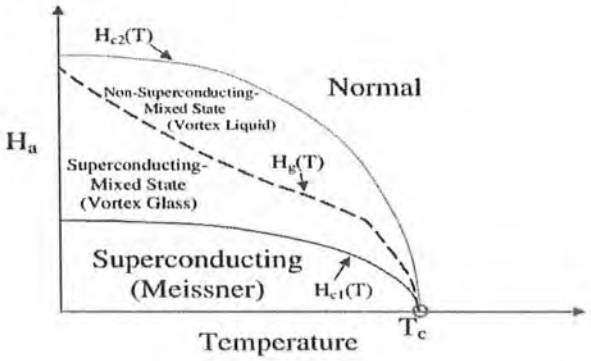

Figure 1-11:Phase Diagram of Type-11 Superconductor

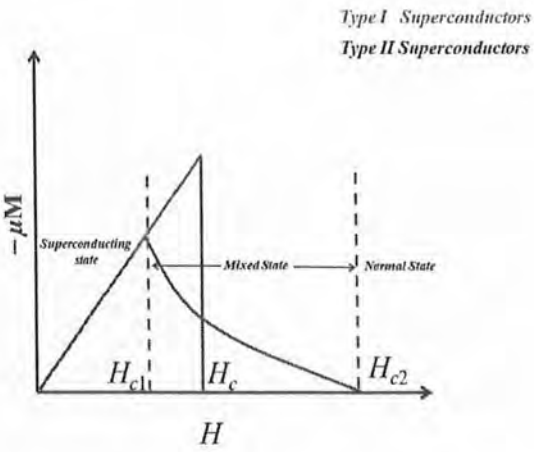

Figure 1-12:Magnetization vs Applied Field

1.3.6 The Bardeen Cooper and Schrieffer (BCS) theory

The first microscopic theory to be put forth was the BCS theory by a Bardeen, a Cooper, and a Schrieffer in 1957[10].The Leon Cooper brought the idea of attractive interactions between electrons that form pairs called Cooper pairs. The mediator that drive the electrons to attract each other are the lattice vibrations or phonons. The electron repels other electron due to their negative charge, but it attracts the positive ions that make up a lattice. But when an electron moves across the positive ions it distorted the lattice from their mean position via attractive potential, increasing the positive charge density in the neighbourhood. The positive charge density attracts another electron. As shown in Fig1-13, the displaced ions allow the attractive forces between the electrons to overcome the repulsive forces of the electrons, allowing them to bound in pairs. Hence the pair of electrons generated via electron phonon interaction having attractive potential between them and behave like composite bosons. These composite bosons which are known as Cooper pairs condensed to form ground state at $T_c(R=0)$ and follow Bose- Einstein statistics.

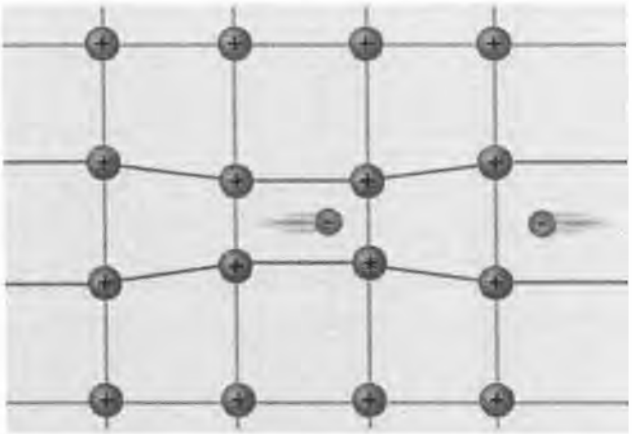

Figure 1-13:Lattice Mediated for the Formation of Cooper Pair

In momentum space, the Cooper pair formed, when one electron emits a phonon of momentum ħq and other absorbed it. This interaction is given by

$$V_{eff} = |g_{eff}| \frac{1}{\omega^2 - \omega_D^2} \qquad (1.23)$$

where $|g_{eff}|$ is a matrix element representing the probability that one electron emits a virtual phonon and a second electron absorbs it, ω is the frequency of electron being considered, and ω_D is the Debye frequency. The negative V_{eff} means attractive potential and it is possible when those electrons near the fermi level take part in attraction whose energies differ from fermi level is less than or equal to Debye energy of lattice ($\hbar\omega_D$).

The attractive interaction of Cooper pair yields a bound state having mathematical expression of energy which is given by

$$|E| = 2\hbar\omega_D e^{-\frac{N(E_f)}{g_{eff}}} \approx 1.76 k_\beta T_c \qquad (1.24)$$

where $N(E_f)$ is a density of the electron states at a fermi level and k_β is a Boltzmann constant and T_c is a critical temperature. The number 1.76 is exact for weak coupling limit and holds true for many but not for all conventional superconductors.

At the critical Temperature Tc(R=0), a condensed state with lower energy than the normal state is formed and hence the band gap appears. The band gap acts as a gateway to normal and superconducting state. The dependence of band gap decreasing with the increase of temperature correctly predicted in case of low temperature superconductors.

This theory is true for conventional superconductor in which electrons and lattice vibration(phonon) interact linearly with each other and their band gap exhibit s-wave symmetry. But in unconventional superconductor the interaction become nonlinear because of strongly correlated medium in which the position and dynamics of each carrier (electron or hole) effect every other carrier immensely. Moreover, appearance of psedogap in a normal state of superconductor is a mystery for BCS theory.

1.4 Thermodynamic Properties

The Second-order phase transition is the change from normal conducting state to superconducting state. Such transition is thermodynamically reversible just like liquid and vapor phase transition. I will discuss below the thermodynamics properties which effect the second order phase transition.

1.4.1 Gibbs Free Energy

The Gibbs free energy in thermal equilibrium is written as.

$$G \equiv U - TS - B.H/4\pi + pV \qquad (1.25)$$

here 'U' is a total internal energy of the system; T is temperature.

S is entropy per unit volume; p is pressure of the system;

H and **B** are applied magnetic field and flux; V is volume,

As $F \equiv U - TS$

so $G \equiv F - B.H/4\pi + pV \qquad (1.26)$

here 'F' is called Helmholtz free energy [26]. The Helmholtz free of a normal state 'Fn' is greater than the value of the superconducting state 'Fs'.

$$F_n - F_s = H_c^2/8\pi \qquad (1.27)$$

This is also called condensation energy and H_c is thermodynamic critical field.

1.4.2 Entropy

Entropy is the defined as disorder of the state. As the electrons of superconducting state are more organized than electrons in normal-state so we can say that entropy of 'S_N' in the normal state is larger than the entropy of 'S_S' in the superconducting state.But at critical temperature both states have same entropy [27]. The difference in entropy between these two states is given by:

$$S_N - S_S = -H_c/4\pi \, (\partial H_c/\partial T_R) \qquad (1.28)$$

So the third law of thermodynamics states that the entropy of a system at T=0K, approaches a limit value 'So' that is independent of all its parameters. SO SN-SS=0 as T=0. At T=Tc, Hc=0 so SN-SS =0. Also $0<T<Tc$, $(\partial Hc/\partial T)<0$, therefore SS<SN meaning that a superconducting state is better organized than normal one.

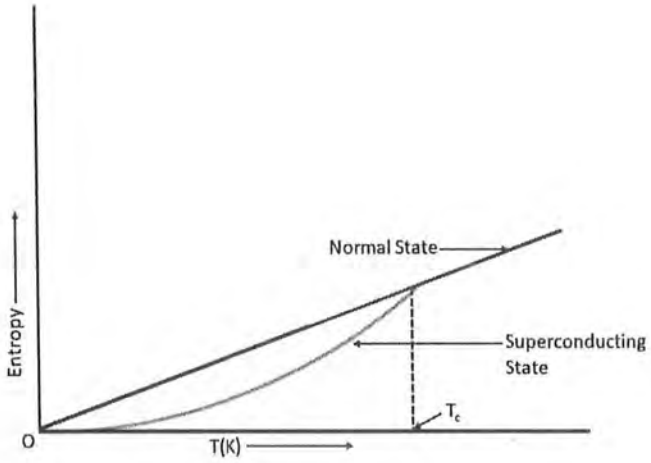

Figure 1-14:Entropy as a Function of a Temperature in the superconducting and the Normal state.

1.4.3 A Specific Heat

Specific heat of a metal consists of electron and lattice contributions.

$$C = C_{el} + C_{lat} \qquad (1.29)$$

From theory of normal metals, at minimum temperature lattice specific heat depends upon temperature that is given as $C_{lat}=\beta T^3$ and $C_{el}=\gamma T$, so;

$$C = \gamma T + \beta T^3 \qquad (1.30)$$

Since the superconducting transition does not effect the lattice, so the lattice specific heat does not change below T_c but electronic specific heat changes drastically below T_c [28].

Therefore, here below a 'Tc', the electronic specific heat falls exponentially with decreasing the temperature.

$$(C_{el})_S = A\exp(-\Delta(T)/K_B T) \qquad (1.31)$$

where 'A' is constant and 'Δ' is energy gap.

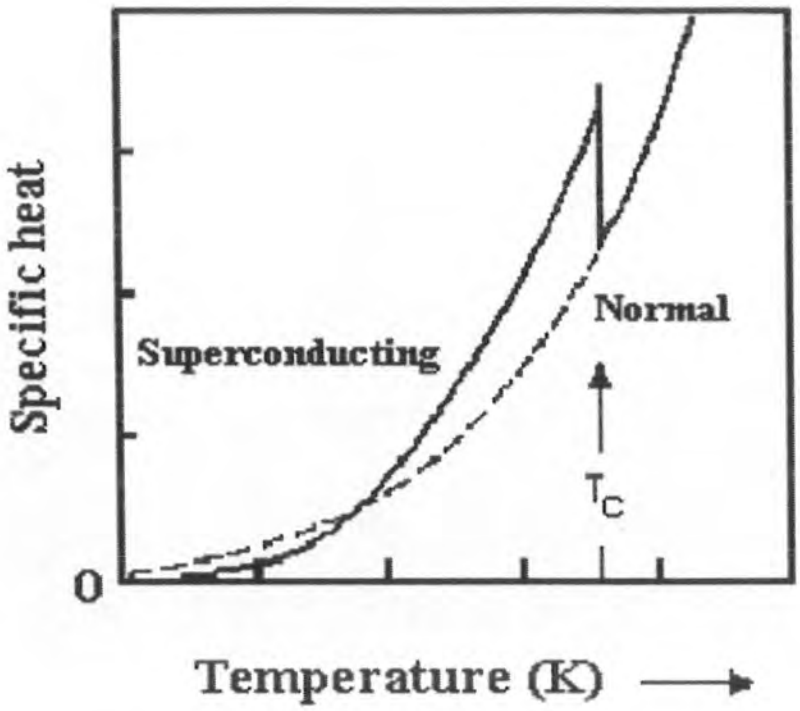

Figure 1-15:Specific Heat as a Function of Temperature

1.5 Dielectric Properties of Superconductors

We analyzed how permittivity changes by changing the frequency, pressure, temperature and shape of the sample.

1.5.1 Capacitor

The device used for storing charge in the electric field is called a capacitor. It contains different conducting and dielectric layers.

1.5.2 Permittivity (Dielectric constant)

Dielectric material have the capability of storing the energy if it is exposed to applied electric field. The quantity of a charge stored in the capacitor increases when dielectric medium is

located within a parallel plate capacitor.The relation between capacitance and dielectric constant is:

$$C=\varepsilon_0\frac{A}{d} \qquad (1.32)$$

here ε_0 is a permittivity of a free space and 'A' is area of a parallel plate of a capacitor and 'd' is a spacing between them.

According to electromagnetic theory, electric displacement or electric flux density D_f is defined as,

$$D_f = \varepsilon E \qquad (1.33)$$

$$\therefore \varepsilon = \varepsilon_0 \varepsilon_r$$

So here 'ε_0' is permittivity of a free space while 'ε_r' is relative permittivity. A complex number called relative permittivity defines how an electric field interacts with a dielectric medium. The real component of the permittivity (ε_r') measures how much energy from an external field may be stored in a material.Whereas imaginary part (ε_r'') tells that how much field dissipates in the dielectric medium? ε_r' is always greater than ε_r''.

1.5.3 Dielectric Loss (tanδ)

The ratio of the imaginary to real parts of the dielectric constant is known as the loss factor.

$$\tan\delta = \varepsilon_r''/\varepsilon_r' \qquad (1.34)$$

It is also named as "tan delta" or "dissipation factor".

1.6 Important Parameters relating Superconductivity

1.6.1 1.6.1 Critical Temperature (Tc)

The resistivity of superconducting composites drops to zero when it is cooled below(12) a specific Temperature.So here this Temperature is called the critical Temperature 'T_c'. BCS theory says that below Tc, two electrons present in the same state hooked up by phonons and hence a Cooper-pair form. This Cooper pair has an integral spin and behaves like a boson. Above Tc, resistance enhances which produces heat. This heat causes the Cooper-pairs to depart and hence the superconductivity of the material gets destroyed.

1.6.2 Critical Field (Hc)

Besides Tc, the critical field also affects the superconductivity of material. Tc and Hc are inversely linked with each other.As the applied magnetic field increases from its acute value, magnetic flux begins to be emitted from the sample (perfect diamagnetism).

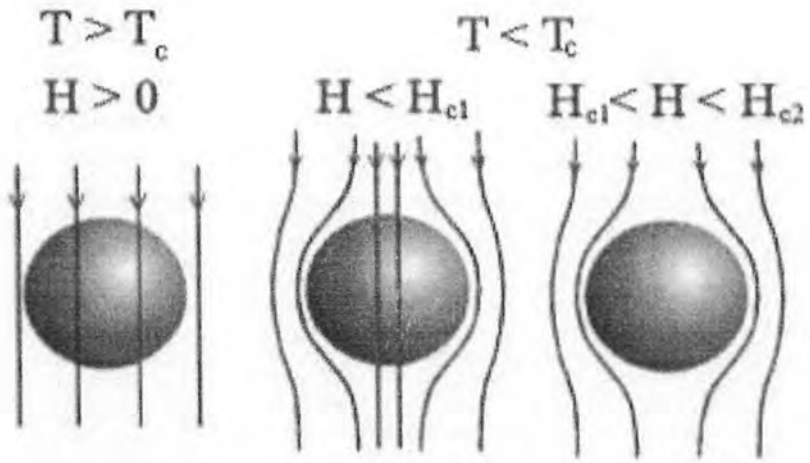

Figure 1-16:Expulsion of Magnetic Field lines from the Material when T<Tc and H>Hc

Critical field is contingent on temperature [14] and is mathematically written as:

$$H_c(T) = H_c(0)\left[1 - (\frac{T}{T_c})^2\right] \qquad (1.35)$$

Where $H_c(0)$ defines the magnetic field at zero kelvin. When $T = T_c$, $H_c(T)$ becomes equal to zero. When the value of H_c is known, then the value of critical current I_c can also be found using the relation:

$$I_c = \frac{2\pi r H_c}{\mu_0} \qquad (1.36)$$

1.6.3 Critical Current Density (Jc)

Superconducting cables can be utilized for conduction of a large amount of current to avoid resistance.

But there are certain limitations on current for flowing through these wires. Current per unit area flowing through superconducting wires is called current density „J". When J > Jc, these wires will not remain superconductors any more i.e. they become normal conductors. Kunzler for the first time observed Jc in 1961. Critical current density is also temperature dependent Jc must have the value higher than 1000 / for practical purposes. Whereas in thallium based cuprate superconductors, 106 to 107 A/cm2 can be achieved at very low temperature.

1.7 High T_c cuprate superconductors

Cuprates superconductors are fall in the category of unconventional superconductors. They are layered compound comprised of CuO_2 planes which are separated by charge reservoir layers as shown in figure 1-17. The charge reservoir layer, which commonly consists of an insulating or semiconducting material, provides charge carriers to the CuO_2 surface. Their crystal structure is usually tetragonal/orthorhombic having space group p4mmm, and they are highly anisotropic because of their d-wave symmetry.

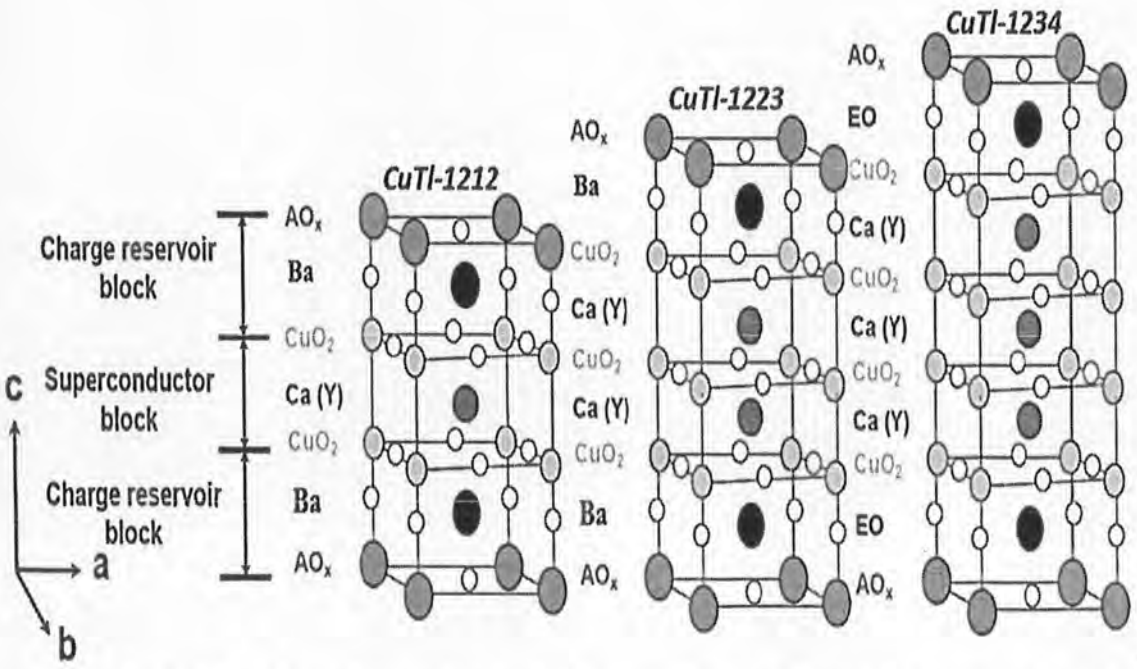

Figure 1-17: The Crystal Structure of some member of the Family of a (CuTl)-Ba-Ca-Cu-O Superconductors.

Anisotropy of a high 'T_c' superconductors decreases as the coupling between CuO planes become strong that leads to the improvement in superconducting properties like T_c, current density, interlayer long range phase coherence etc. The scientists are continuing to pursue superconducting material that exhibit higher critical temperature and low anisotropy. Tl-1223 superconductor one of the members of Tl-Ba-Ca-Cu-O family is anisotropic and has higher $T_c(0)$ than the other single layer of Tl-O material, but due to carcinogenic nature of Tl it has a severe effect on health. Pursuing a material of high T_c a new family of cuprate $CuBa_2Ca_{n1}Cu_nO_{2n+2}$ [Cu-12(n-1)n] (n=1,2,3...) was discovered. It forms under pressures of 4-6 GPa and was thought to be best known for its higher critical current density and critical temperature [29]. They have the same structure as that of Tl based superconductors, but in these compounds, there exist a copper (Cu) in charge reservoir layer ($CuBa_2O_{4n+\delta}$). The family exhibit low anisotropy than Tl family because of their conducting charge reservoir layer. A new subfamily, abbreviated as $Cu_{1-x}Tl_x$-12(n-1)n was discovered by substituting 'Tl' for 'Cu' in Cu-12(n-1)n compounds. This new subfamily exhibits the same properties as Cu-based superconducting materials and can be manufactured at both high and low pressures [30-31]. They have a semi-insulating charge storage layer of $Cu_{1-x}Tl_xBa_2O_{4n-\delta}$ which slightly raises anisotropy (γ=5) but keeps it below that of Tl-based compounds. The crystal structure of members of this family is shown in figure 1-17. The CuO_2 planes separated by Ca atom. While Ba atom act as a bridge between the CuO_2 planes.

1.8 Applications

There are wide range of applications of superconductivity some of them are.

- A SQUID, a form of magnetometer that measures extremely small magnetic fields of the scale of 10^{-18} Tesla, is a superconducting quantum interference device.
- As a powerful electromagnetic it is used in fusion reactors to confine plasma, magnetic levitation (maglev) train, magnetic resonance imaging (MRI), particle accelerators (e.g. Large Hadron Collider) as a magnet that focussing charge particles on the target.

- As a low loss powerful electric cable. Germany manufactured superconducting wire that transmit and distribute power of 10kV at 1km. The wire cooled down to superconducting state by using liquid nitrogen.
- As an electric filter like RF (radio filter) and microwave filter.

1.9 References

[1] M. Tinkham, Introduction to Superconductivity, 2004.

[2] D. van Delft, Phys. C Supercond. 479 (2012) 30–35.

[3] W. Meissner, R. Ochsenfeld, Naturwissenschaften 21 (1933) 787–788.

[4] C. Gorter, H. Casimir, Physica 1 (1934) 306–320.

[5] L. Shubnikov, I. Nakhutin, Nature 139 (1937) 589–590.

[6] Abrikosov, A. A., Sov. Phys. JETP 5 (1957) 1174–1182.

[7] V. Ginzburg, On Superconductivity and Superfluidity: A Scientific Autobiography, 2008.

[8] E. Maxwell, Phys. Rev. 78 (1950) 477–477.

[9] C.A. Reynolds, B. Serin, W.H. Wright, L.B. Nesbitt, Phys. Rev. 78 (1950) 487–487.

[10] J. Bardeen, L.N. Cooper, J.R. Schrieffer, Phys. Rev. 108 (1957) 1175–1204.

[11] B.D. Josephson, Phys. Lett. 1 (1962) 251–253.

[12] A.D. LS Brizhik, Low Temp. Phys. 10.4 (1984) 358–366.

[13] P.W. Anderson, Science. 288 (2000) 480–482

[14] A.S. Davydov, Phys. Rep. 190 (1990) 191–306.

[15] A.S. Davydov, J. Biol. Phys. 18 (1991) 111–125.

[16] V.J. Emery, S.A. Kivelson, Nature 374 (1995) 434–437.

[17] A. Mourachkine, J. Low Temp. Phys. 117 (1999) 401–405.

[18] A. Mourachkine, Europhys. Lett. 55 (2001) 86–92.

[19] J. Rossat-Mignod, L.P. Regnault, C. Vettier, P. Bourges, P. Burlet, J. Bossy, J.Y. Henry, G. Lapertot, Phys. C Supercond. 185–189 (1991) 86–92.

[20] A. Mourachkine, High-Temperature Superconductivity in Cuprates: The Nonlinear Mechanism and Tunneling Measurements, 2002.

[21] Misra, Prasanta. Physics of condensed matter, Academic Press, 2011.

[22] J.G. Bednorz, K.A. Muller, Zeitschrift Fur Phys. B Condens. Matter 64 (1986) 189–193.

[23] M.K. Wu, J.R. Ashburn, C.J. Torng, P.H. Hor, R.L. Meng, L. Gao, Z.J. Huang, Y.Q. Wang, C.W. Chu, Phys. Rev. Lett. 58 (1987) 908–910.

[24] Z.Z. Sheng, A.M. Hermann, Nature 332 (1988) 138–139.

[25] T.W. HUANG, M.P. HUNG, T.S. CHIN, H.C. KU, S.E. HSU, Mod. Phys. Lett. B 04 (2004) 885–893.

[26] A.P. Drozdov, M.I. Eremets, I.A. Troyan, V. Ksenofontov, S.I. Shylin, Nature 525 (2015) 73–76.

[27] M. Somayazulu, M. Ahart, A.K. Mishra, Z.M. Geballe, M. Baldini, Y. Meng, V. V. Struzhkin, R.J. Hemley, Phys. Rev. Lett. 122 (2019) 027001.

[28] V. V. Schmidt, P. Müller, A. V. Ustinov, The Physics of Superconductors : Introduction to Fundamentals and Applications, Springer Berlin Heidelberg, 1997.

[29] H. Ihara, K. Tokiwa, H. Ozawa, M. Hirabayashi, A. Negishi, H. Matuhata, Y.S. Song, Japanese journal of applied physics 33.4A (1994): L503.

[30] H. Ihara, K. Tanaka, Y. Tanaka, A. Iyo, N. Terada, M. Tokumoto, M. Ariyama, I. Hase, A. Sundaresan, N. Hamada, S. Miyashita, K. Tokiwa, T. Watanabe, Phys. C Supercond. 341–348 (2000) 487–488.

[31] T. Kawashima, Y. Matsui, E. Takayama-Muromachi, Phys. C Supercond. 224 (1994) 69–74.

CHAPTER-02
2 LITERATURE REVIEW

In 1988, Z. Z. Sheng et al. [1] for the first-time discovered family of thallium-based superconductors (Tl–Ba–Cu–O). This family showed zero resistance critical temperature Tc(R=0) above 90K and revealed that by substitution of different elements may increase the Tc(R=0) higher than the parent compound. They also reported that the substitution of Ba at Ca site increase Tc(R=0) higher than 100 K and show onset temperature of 120 K. Moreover, they claim that the superconductor they discovered is more stable and reproducible.

Parkin et al. [2] reported zero resistance critical temperature ranges between 118 K and 127 K in $Tl_2Ba_2Ca_2Cu_3O_x$ superconductor. They revealed that variation in Tc(R=0) depends upon the processing condition. They concluded from transmission electron spectroscopy that unit cell of $Tl_2Ba_2Ca_2Cu_3O_x$ superconductor exhibit body-cantered tetragonal structure which further comprised of trilayer copper perovskite block linked through bilayer thallium oxide block.

D. Tristan et al. [3] prepared $Tl_2Ba_2Ca_2Cu_3O_{10+x}$ and $Tl_2Ba_2Ca_3Cu_4O_{12+x}$ using a diamond anvil cell under high pressure up to 21 GPa. They used four probe method developed by Van Eenige et al [4] for high pressure experiments to measure resistance. At ambient pressure, they have zero resistance critical temperatures of 128.5 and 113 kelvin(k) respectively. but due to increase in pressure the Tc (R=0) continues to increase up to 133 K under 4.2 Gpa for $Tl_2Ba_2Ca_2Cu_3O_{10+x}$ and 120 K under 6.6 GPa in $Tl_2Ba_2Ca_3Cu_4O_{12+x}$.

H. Ihara et al. [5] successfully synthesized single layered thallium oxide superconductor having chemical formula $TlBa_2Ca_{n-1}Cu_nO_y$ (n = 3 and 4). The phases of single layered TlO superconductors are unstable and difficult to synthesis than double layer but these materials possess relatively higher critical temperature and current density so that they are more reliable from application point of view than double layer. In order to overcome phase instability, they substitute Sr at Ca site and Pb or Bi at Tl site. They note that the greatest obstacle to the creation of the $TlBa_2Ca_{n-1}Cu_nO_y$ (n = 3 and 4) phases is the presence of carbon impurities.

E. Ohshima et al. [6] achieved almost single phase $TlSr_2Ca_2Cu_3O_x$ by apply pressure of 2.5 GPa without any elemental substitution. They synthesized their sample at 1000 C for 4 hour and

reported Tc = 97 K by using SQUID. From X-ray Diffractometer (XRD) analysis they found their sample exhibit tetragonal structure. They concluded that the high pressure urges Tl not to evaporate while at ambient pressure thallium oxide escape out during synthesis that caused long ordered structural instability in the formation of $TlSr_2Ca_2Cu_3O_x$.

K. Tokiwa et al. [7] claim Tc≈130 K in their $(Cu_{0.5}Tl_{0.5})Ba_2Ca_2Cu_3O_x$ (CuTl 1223) samples at ambient temperature and further investigate the effect on Tc under pressure of 8 GPa via cubic anvil cell. XRD analysis reflect single phase of CuTl 1223 superconductor. They used four probe method and conclude that the onset temperature is increased from 134.6 K to 147.0 K under pressure of 8 GPa.

Bulk their $(Cu_{0.5}Tl_{0.5})Ba_2Ca_2Cu_3O_x$ superconductor was created by N. Khan et al. [8] using a straightforward solid state chemical technique.They grind a Cu(CN), a $Ba(NO_3)_2$ and a $CaCO_3$, by the use of mortar and pestle following the firing at 840 C. After firing, Tl_2O_3 mixed with sample to formed pellets. These pellets enclosed in aluminium foil and they heated them for 30 min. After post annealing in nitrogen environment they found onset Tc at 110 K and Tc(R=0) at 103 K via four probe resistivity measurement method. The FTIR absorption measurement reflect optimum doped material.

N. Khan et al. [9-10] conceived an idea of a substitution of Mg/Be at the Ca site in different ratios in $(Cu_{0.5}Tl_{0.5})Ba_2Ca_2Cu_3O_{10-\delta}$. The parent compounds they utilised in synthesis of $(Cu_{0.5}Tl_{0.5})Ba_2Ca_2Cu_3O_{10-\delta}$ (where x = 0, 0.5, 1, 1.5) were CuCN, MgO, $Ca(NO_3)_2$ and $Ba(NO_3)_2$. These compounds were correctly ground for an hour using the solid state reaction technique and fired in a quartz boats by setting temperature at 840 C. After first firing they grind them again and kept the sample for second firing in a furnace. At the end Tl_2O_3 mixed via grinding that leads to the formation of resultant compound i.e. $Cu_{0.5}Tl_{0.5}Ba_2Ca_{2-x}Mg_xCu_3O_{10-\delta}$ (where x = 0, 0.5, 1, 1.5). The resultant compound pelletized enclosed in a foil of aluminium and sintered for 10 min. They report a systematic behaviour of increasing Tc against doping of Ca at different ratio. After using four probe resistivity measurements they found that for x = 0 composition observed Tc(R = 0) = 82 K and for x = 1.5 it was 92 K. They conclude from their results that increased in Tc(R=0) occur due to doping of more electronegative Mg at less electronegative Ca site that causes the displacement of electron clouds of Cu towards Mg, which could be the possible reason for shortening of c axis length, reflected from XRD analysis. They also did FTIR measurement and

found softening of apical modes to lower wave number which further strengthened their conclusion.

N. A. Khan et. al. [11] synthesized the samples of $Cu_{0.5}Tl_{0.5}Ba_2Ca_2Cu_{3-x}Zn_xO_{10-\delta}$ (x = 0.75,1.5,2.25,2.65) by two-step solid-state reaction technique and reported that substitution of Zn at Cu planar site enhanced superconducting properties. The XRD analysis showed tetragonal structure and reduction in the c axis length by substitution of Zn in different ratio. By four probe resistivity measurement increasing order in resistivity reported against concentration of Zn substitution. The highest T_c is 121 K observed for x= 2.65. Bulk diamagnetic nature was confirmed by ac susceptibility measurement which point out their increasing trend against increasing concentration of Zn. FTIR analysis reflect softening of phonon modes of apical oxygen to lower wave number and unchanged behaviour of in planar oxygen modes for different concentration of Zn.

N. L. Wu. et al. [12] adapted powder synthesis method to prepare $Tl_2CaBa_2Cu_2O_8$ (2122) and $Tl_2Ca_2Ba_2Cu_3O_{10}$ (2223) superconductors. For the sake of preparation, they used stoichiometric mixture of Tl_2O_3, CuO and $CaBa_2CuO_4$ for both of their samples but for 2223 they used CaO and CuO as an additional reactant to satisfy stoichiometry. After calcination of sample 2122 at 830° C for a period of 14hour, a four-probe method employed to measure critical temperature Tc (R = 0). The Tc (R=0) found was 116 K. There XRD analysis reflect single phase formation of their sample with minimum impurities phases. For 2223 sample they performed calcination in two steps to get single phase with minimum impurities phases. In first step the calcination occurred at 830° C for five hours while in second step it occurred at 870° C in the time domain of 2 to 6 hours. From four probe method they found Tc (R = 0) between 110 and 118 K. Both of their samples show abrupt transition and showed a saturated Meissner effect of 20 percent when placed in the magnetic field of 20 G. The main problem with given method is powder melting that leads to extensive loss of thallium during calcination, and formation of impurities that did not show superconducting behaviour.

M. Rafique et al. [13] doped carbon nanotube in CuTl-1223 superconductor at different weight percent (0 to 7 wt. %). Their samples were created using a two-step solid-state reaction process. They characterized their sample using XRD, four probe resistivity apparatus, and scanning electron microscopy (SEM). From XRD analysis their sample showed orthorhombic

structure having of single phase. A small variation in c axis length was observed from 0.27 to 0.20 Å, which possibly point out the intercalation of carbon atoms from carbon nanotubes in the unit cell. The SEM analysis of their sample showed intergrain connectivity via carbon nanotubes that enhance intergranular current flow. From fluctuation induced conductivity (FIC) analysis the shrunken of 3D regime and suppression of superconducting properties like coherence length, fermi velocity, and coupling constant reported against the concentration of carbon nanotubes. They describe the reason that carbon atom from carbon nanotubes diffused into the unit cell that acted as a columnar defect having nonsuperconducting nature and caused the suppression of superconducting parameter.

R. K. Nkum et al. [14] studied superconducting properties of indium doped $Bi_{1.84}Pb_{0.34}Sr_{1.91}Ca_{2.03}Cu_{3.06}In_xO_y$ samples at room temperature. They characterized the samples using a four-probe method for resistance measurements and Wayne Kerr digital LCR mete for dielectric measurement. They used conventional solid-state method and shaped their sample in the form of pellets. They investigated an electrical resistivity, a dielectric constant, the carrier concentration, and the tangent loss against the concentration in indium. They found that increase in indium concentration leads to increase in dielectric constant which reflect the enhancement of polarization in the sample. On the other hand, loss tangent, that tell us about the losses in Bi based sample, and carrier concertation, decreased with increasing concentration of indium. The resistivity increases as the carrier concentration decreases of sample probably due to localization of charge carrier and, magnetic disorders in CuO_2 plane.

S. Cavdar et al. [15] studied dielectric properties of $Tl_2Ba_2Ca_2Cu_3O_x$ (Tl2223) and $Tl_2Ba_2Ca_1Cu_2O_x$ (Tl 2212) samples. They synthesized their samples in the form of pellets. Afterward they characterized them by using X-ray diffractometer for structural analysis, four probe method for resistivity measurement, and impedance analyser for dielectric measurement. The resistivity measurement shown T_c^{offset} and T_c^{onset} at 112 K and 125 K respectively. The difference in T_c^{offset} and T_c^{onset} was around 13 pointed out that samples may have two phases which was also confirmed from their XRD pattern. The dielectric measurement include real and imaginary part, tanδ losses, and ac conductivity. They investigate the behaviour of negative capacitance, a dielectric constant, conductivity, and the tangent loss of their sample with a temperature, and frequency. By maintaining the frequency down in the range of 7 kHz to 2 MHz, the actual part of

the dielectric constant enhanced with increasing temperature. Their increasing behaviour attribute to enhancement of dipolar polarization. At higher frequency (2–10 MHz) they reported no significant change in real component of a dielectric constant with temperature and an imaginary component of a dielectric constant depicts the increasing behaviour with decreasing frequency, and temperature while their dispersion is weaker than that of real part. The tanδ losses shows abrupt decreasing trend at low frequency but constant behaviour at higher frequency. They reported that ac conductivity shown linear relation with logarithmic frequency in the range of 105–106 Hz which indicate hooping of charge carrier. At lower frequency range i.e. less than 100 kHz no appreciable change accountant in their behaviour at all temperature. An increasing fashion of ac conductivity reported with decreasing temperature and frequency.

The impact of Zn doping on $Cu_{0.5}Tl_{0.5}Ba_2Ca_2Cu_{3-x}Zn_xO_{10-\delta}$ (x =0.75,1.5,2.25,2.65) samples was investigated by N. Khan et al. in their study [16]. They used two-step solid-state reaction technique and synthesized their sample in the form of pellets. They characterised their sample by measuring resistivity with four probes-method, mutual inductance method for ac susceptibility, and LCR meter for dielectric measurement. The dielectric measurement includes a real and an imaginary part of the dielectric, tanδ losses, and the ac-conductivity. With increased Zn doping, a systematic rise in the zero resistivity critical temperature was seen through measurements of resistivity and ac-susceptibility, which in turn improved the diamagnetic character of their samples. The dielectric response was measured at frequencies ranging from 10 kHz to 10 MHz and found that at a lower frequency '10kHz' real part of dielectric enhanced with increasing concentration of Zn which leads to decreased in tanδ loss at 79 K as well as at room temperature. They argue that enhancement in real part of dielectric parameter is due to increasing concentration of charge carrier that leads to enhanced density of polarization. They reported suppression of an imaginary component of the dielectric constant with increasing the frequency at '79 K' and at room temperature. On the other hand, the decreasing behaviour also reported with increasing Zn doping probably due to the lower conductance of a Zn and because of the filled 3d10 shell, the semiconductor has a wide band gap, as compared to metallic Cu having partially filled $3d_9$ shell. The ac conductivity shows increasing trend at frequency up to 2 MHz with Zn doping reflected enhanced charge carrier. But at greater than 2 MHz they observed that conductivity leads to normal state value.

A. Younis et. al [17] studied different properties of $Cu_{0.5}K_{0.25}Ba_2Ca_3Cu_4O_{12-\delta}$ sample. They synthesized their sample by two-step solid-state reaction technique and shaped them in the form of pellets. Afterward they characterized their sample by using four-probe method for the resistivity measurement, mutual inductance method for ac susceptibility, and LCR meter for dielectric measurement. At 101 K, they reported a zero resistivity critical temperature Tc(R=0). Diamagnetic nature of their sample was reflected from susceptibility measurement. They found that the negative value of the real part of the dielectric constant was attributed to the negative capacitance exhibited by the sample. The negative values are suppressed as the frequency and measured temperature values increase,probably due to decrease in polarization density. With rising frequency and temperature, the imaginary portion of the dielectric constant has a tendency to decrease. They observed gradually increased in negative values of tanδ losses with measured temperature while increasing trend reported with increased in frequencies. The ac conductivity decreased by increasing temperature and indicated saturation at low frequencies at all measured temperature.

M. Mumtaz et. la [18] added nickel nanoparticles in a $(Cu_{0.5}Tl_{0.5})Ba_2Ca_2Cu_3O_{10-\delta}$ of superconducting matrix having concentration of x=0–1.00 wt.%.The solid state reaction method was used to create the phases of $(Cu_{0.5}Tl_{0.5})Ba_2Ca_2Cu_3O_{10-\delta}$ superconductor while for the nanoparticles a method known as sol-gel method was adapted. e dielectric properties were investigated using an LCR metre with a frequency range of 10kHz to 10MHz and temperatures ranging from 78 to 290 kelvin(k).A dielectric measurement includes real and imaginary part, tanδ losses, and ac conductivity. The real part points out energy stored in a sample while imaginary part reflects dissipation of energy in the presence of external applied field. Their graphical results show steady decrease of real part towards zero value with increase in frequency pointed out that the time period of polarization would be greater than that of external ac signal. Suppression in real part of dielectric was reported up to x = 0.72 wt.% and higher values were observed at maximum concentration of x = 1.00 wt.%. The reason of increased in value reflected increase in the number of charge carrier ensnared at grain boundaries. The imaginary part showed higher values at the lower frequency and afterward gradually decrease in a frequency. A behaviour reflected that at lower frequency of ac signal charge carriers flow but as the frequency was increased time period of polarization become greater than that of ac signal that resulted decrease in flow of charge carriers. With the addition of Ni nanoparticles imaginary part of dielectric constant first decrease and then began to increase with Ni concentration at all temperature. Higher values reflect higher

energy losses due to barriers of high potential formed by Ni nanoparticles. A peak was observed in tanδ loss graph that pointed resonance phenomena occur due to superposition of applied frequency with carrier's frequency. Higher values of ac conductivity reported against frequency that reflected enhanced condition of hooping electron at all temperature.

X. Xu et al. [19] studied different superconducting properties of $Bi_2Ba_2Nd_{1.6}Ce_{1.4}Cu_2O_{10+\delta}$ compound. They prepared their sample by using a solid-state reaction technique.in the interest of purity, the reaction, of a formation of resultant compound, was carried out in vacuumed which minimized the phases of Bi oxide which act as an impurity. Afterward they baked their sample and shaped them in pellets. They characterized their sample by using X-ray Diffractometer for structural analysis, and LCR meter for dielectric measurements in the 80-300 K and 20-106 Hz temperature and frequency ranges. The dielectric measurement includes real and imaginary part, tanδ losses, and ac conductivity. X ray analysis show orthorhombic structure of their sample. The dielectric permittivity shows decreasing trend with temperature at all measured frequencies. While at low frequency of 10 Hz it was almost exponentially increasing with temperature. They reported that dielectric permittivity shows high values at low a frequency and a room temperature compared to the values at the high frequency and at the low temperature. At high frequency of 106 Hz no changed in dielectric permittivity reported at all temperature because of negligible contribution from dipolar polarization. They studied loss tanδ measurement and reported shifting of peak toward high temperature with increasing frequency. The peaks reflected maximum dissipation which point out the occurrence of resonance between applied frequency and dipolar frequency while shifting of peaks towards higher temperature were due to relaxation time that decrease with increasing te

$Cu_{0.5}Tl_{0.5}Ba_2Ca_3(Cu_{4-x}Cd_x)O_{12-\delta}$ (x =0,0.25,0.5,0.75 samples were examined by M. Raheem et al. [20] to determine the impact of Cd doping at the Cu site. They used a two-step solid state reaction technique to create their $Cu_{0.5}Tl_{0.5}Ba_2Ca_3(Cu_{4-x}Cd_x)O_{12-\delta}$ (x =0,0.25,0.5,0.75) and then formed them into pellets. They characterized their sample by using X-ray Diffractometer for structural analysis, four probe method for resistivity measurement, mutual inductance method for ac susceptibility, and LCR meter for dielectric measurement that included real and imaginary, tanδ losses, and ac conductivity. The XRD analysis shown tetragonal structure of their sample with increasing c axis length against the concentration of Cd. The zero-resistivity critical temperature

decreased with Cd concentration due to damped harmonic oscillation of Cd atom having mass greater than that of Cu in CuO2 planes. This leads to limit the population of electron phonon interaction, resulted in suppression of superconducting properties. The real part of dielectric points out energy stored in a sample while imaginary part reflects dissipation of energy in the presence of external applied field. The real part of dielectric constant indicated negative values because of negative capacitance and moved gradually towards zero values with applied frequencies at all temperature. The decreased in magnitude of real part of dielectric constant attributed to an-harmonic oscillation of heavier Cd atom that reduced polarization density. The imaginary part of their samples indicated decreasing trend with increasing frequency, and temperature. The tanδ losses show increased in values with temperature in all Cd doped sample. The lower losses in Cd doped samples pointed out the presence of Cd atom around defects and grain boundaries. The ac conductivity indicated decrease in values with decreased in temperature reflected lower cross section of charge carriers. In Cd doped sample the lower values of ac conductivity pointed decreasing population of electron phonon interactions.

I. Younes et. al [21] studied dielectric properties of $(CH)_{nx}$ / $(Cu_{0.5}Tl_{0.5})Ba_2Ca_3Cu_4O_{12-\delta}$ samples having different concentration levels ($0 \leq x \leq 0.1$ wt. %) of graphene. They synthesized their samples by conventional one-step solid-state reaction method and then formed them into pellets. They characterized their sample by using X-ray Diffractometer for structural analysis, four probe method for resistivity measurement, FTIR measurement between 400–700 cm-1 that was done to study change in oxygen mode with addition of graphene, mutual inductance method for ac susceptibility, and LCR meter for dielectric measurement that includes real and imaginary part, tanδ losses, and ac conductivity. From XRD analysis the lattice parameter shown unsystematic variation at different concentration of graphene. From which they conclude that addition of graphene did not change the structure of the crystal instead it fill the voids between the grains. The optimal concentration was found to x = 0.04 wt% while high concentration hindered the formation of required phases. The increased in zero resistvity critical temperature was reported pointed out increase in conduction between grains that linked with each other through accumulation of graphene at voids. The FTIR measurement shown variation in apical as well as in planar mode signifies the stress and strain of added graphene brought change in bonding of oxygen. The decreasing values of a real part of the dielectric constant in frequency at all the temperature attributed to decrease in population of dipolar polarization density. At frequency higher than 1

MHz their dependence on temperature become insignificant pointed the contribution of electronic and lattice polarization. The imaginary part show the same behaviour as that of real part and described according to a Maxwell– Wagner model and a Koop's phenomenological theory. These models based on the argument that dielectric material comprise of two parts one is conductive grain with large permittivity and other is boundaries of grain with comparatively low permittivity. The latter shown higher response at low frequency than the former one and had maximum value at x = 0.10 wt.% possibly, due to agglomeration of graphene at grain boundaries. The tanδ losses reported decreasing trend with frequency at all temperature and agreed with the result of SEM. The results shown the significant increase in properties of superconducting state till x = 0.04 wt.% above which it diminished with the accumulation of graphene high concentration. The increase in ac conductivity at 110 K with addition of graphene signified the weak links among grains in crystal.

N. Khan et. al [22] investigated a dielectric response of $Cu_{0.5}Tl_{0.5}Ba_2Ca_2Cu_{3-x}M_xO_{10-\delta}$ (M = Cd, Zn, Ni; x = 0, 1.5) superconducting compounds. They used two-step solid-state reaction technique and synthesized their sample in the form of pellets. They characterized their sample by using X-ray Diffractometer for structural analysis, four probe method for resistivity measurement, mutual inductance method for ac susceptibility, FTIR measurement between 400−700 cm-1, and LCR meter for dielectric measurement that included real and imaginary part, tanδ losses, and ac conductivity. The XRD analysis shown orthorhombic structure with increasing c axis length in all the doped samples. A zero-resistivity critical temperature decreased with Cd doped while it increased in case of Ni and Zn doping.Ac-susceptibility is suppressed in all doped samples, with the greatest suppression found in Cd doped samples.In all doped sample the negative values of real, and positive values of imaginary component of a dielectric constant suppress a increase in frequency at all temperature. A maximum suppression reported in Cd doped sample arises due to a harmonic oscillation in CuO2 /CdO2 plane. The tanδ losses shown resonance peak in all doped and undoped sample arises due to the matching of applied frequency and polarization frequency of interfaces. They reported decreasing trend in ac conductivity within increase in frequency and temperature.

2.1 References

[1] Z.Z. Sheng, A.M. Hermann, Nature 332 (1988) 138–139.

[2] S.S.P. Parkin, V.Y. Lee, E.M. Engler, A.I. Nazzal, T.C. Huang, G. Gorman, R. Savoy, R. Beyers, in: Springer, Dordrecht, 1988, pp. 309–312.

[3] T.W. Huang, M.P. Hung, T.S. Chin, H.C. Ku, S.E. Hsu, Mod. Phys. Lett. B 04 (2004) 885–893.

[4] E.J. E. N. van Eenige, R. Griessen, R. J. Wijngaarden, J. Karpinski, E. Kaldis, S. Rusiecki, Phys. C 168 (1990) 482–493

[5] H. Ihara, K. Tanaka, Y. Tanaka, A. Iyo, N. Terada, M. Tokumoto, M. Ariyama, I. Hase, A. Sundaresan, N. Hamada, S. Miyashita, K. Tokiwa, T. Watanabe, Phys. C Supercond. 341–348 (2000) 487–488.

[6] E. Ohshima, T. Atou, M. Kikuchi, Y. Syono, Phys. C Supercond. Its Appl. 282–287 (1997) 827–828.

[7] K. Tokiwa, H. Aota, C. Kunugi, K. Tanaka, Y. Tanaka, A. Iyo, H. Ihara, T. Watanabe, Physical Review, B 63.6 (2001) 064508.

[8] N.A. Khan, Fasih-ud-Din, A.A. Khurram, Phys. C Supercond. Its Appl. 417 (2005) 119–126.

[9] N.A. Khan, A.A. Khurram, Appl. Phys. Lett. 86 (2005) 1–3.

[10] N.A. Khan, G. Husnain, Phys. C Supercond. Its Appl. 436 (2006) 51–58.

[11] N.A. Khan, M. Mumtaz, Supercond. Sci. Technol. 19 (2006) 762–766.

[12] S.-Y.W. a and E.R. c Nae-Lih WU a, Yeong Der YAO b, Sern-Nan LEE a, Phys. C 161 (1989) 302–312.

[13] M.A.R. · S.A. · N.H. · N.A.K. Khan, J Supercond Nov Magn 27.11 (2014) 2427–2434.

[14] R.K. Nkum, M.O. Gyekye, F. Boakye, Solid State Commun. 122 (2002) 569–573.

[15] Ş. Çavdar, H. Koralay, N. Tuğluoğlu, A. Günen, Supercond. Sci. Technol. 18 (2005) 1204–1209.

[16] N.A. Khan, M. Mumtaz, A.A. Khurram, J. Appl. Phys. 104 (2008) 033916.

[17] A. Younis, N.A. Khan, Mod. Phys. Lett. B 24 (2010) 3097–3107.

[18] M. Mumtaz, M.A. Asghar, Low Temp. Phys. 44 (2018) 759–764.

[19] X. Xu, Z. Jiao, M. Fu, L. Feng, K. Xu, R. Zuo, X. Chen, Phys. C 417 (2005) 166–170.

[20] M. Rahim, N.A. Khan, M. Mumtaz, J. Low Temp. Phys. 172 (2013) 47–58.

[21] I. Younes, H. Basma, M. Anas, R. Awad, Mod. Appl. Sci. 13 (2019) 12–18

[22] N.A. Khan, A. Saba, A. Raza, J. Alloys Compd. 757 (2018) 476–483.

CHAPTER-03
3 SAMPLE PREPARATION AND EXPERIMENTIAL TECHNIQUES

This chapter contains the information about the preparation for a $Cu_{0.5}Tl_{0.5}Ba_2Ca_2(Cu_{3-x}Cs_x)O_{10-\delta}$ (x=0,0.5,1,1.5,2,2.5,3) samples of a superconductors. Synthesis of samples and different characterization tools which are used during the current work will be explained in detail. Later on different experimental techniques will be discussed in detail given below to study the dielectric, electrical, structural and optical properties of pure CuTl-1223 samples.

3.1 Synthesis Technique

Different methods are used for production of high Tc superconductors but the most simplest method used in the present work for the synthesis of ceramic material is a solid state thermochemical reaction. So a Solid state reaction methods were used for a production of our samples as it is economically low and suitable to use as compared to other methods because of performance and reliability.

3.1.1 Solid State Reaction Method

In this process solid materials are used as precursor for the preparation of polycrystalline solids. Reactants surface area, structural properties, reactivity and different reaction conditions are responsible for the reaction rate.All the chemicals were taken in a fixed ratio and then grinded for one and a half hour for better mixing and to enhance the contact between the reactants. After grinding the mixed material was heated at high temperature (860oC) because 31 considerable amount of energy is needed to overcome precursor's lattice energy. This high temperature helps the movement of atoms at a sufficiently high rate to obtain the required product. The movement of atoms through the solid lattice is a slow process and if the temperature is increased significantly then rapid migration of atoms is possible. The solid state reaction consists of two main stages, calcination and sintering. In calcination the chemicals are decomposed (breaking of solid oxides) and combine again to give new compounds. In the second stage thallium mixed pallets were heated

for 10 minutes by using gold capsule. Grain size and crystallinity of the product is improved in sintering process.

3.1.2 Synthesis of Samples

Using a solid state reaction technique, $Cu_{0.5}Tl_{0.5}Ba_2Ca_2(Cu_{3-x}Cs_x)O_{10-\delta}$ for (x=0.5,1,1.5,2,2.5,3) superconducting samples were created. Barrium nitrate, calcium carbonate, copper cyanide, Cesium Carbonate and thallium oxide were used for the synthesis of our samples.

In the initial stage, barium nitrate, calcium carbonate, copper cyanide, and Cesium Carbonate were mixed in appropriate proportions and properly ground in a quartz mortar and pestle for 1.5 hours. The quartz boats were then filled with this substance and placed in a preheated chamber furnace for 24 hours at 860°C. The chamber was then turned off and allowed to cool to room temperature. So the precursor was once again ground for 1.5 hours and heated for 24 hours in a furnace.

So in the second stage the overheated material was combined with a calculated amount of Tl_2O_3 ground for 45 minutes in a quartz mortar and pallets were made by applying 4 tons/cm2 pressure using hydraulic press. Then, these pallets were covered in gold capsules for sintering and kept in a chamber that had been preheated to 860°C for ten minutes. Following the heat treatment, the pallets were quenched at room temperature to obtain the final $Cu_{0.5}Tl_{0.5}Ba_2Ca_2(Cu_{3-x}Cs_x)O_{10-\delta}$ (x=0.5,1,1.5,2,2.5,3) Composites

Serial No	Chemicals	Formula
1	Barium Nitrate	$Ba(NO_3)_2$
2	Calcium Carbonate	$CaCO_3$
3	Copper Cyanide	$Cu_2(Cn)_2.H_2O$
4	Calcium Carbonate	Cs_2CO_3
5	Thallium Oxide	Tl_2O_3

Table 3-1:Chemicals used for Sample Preparation

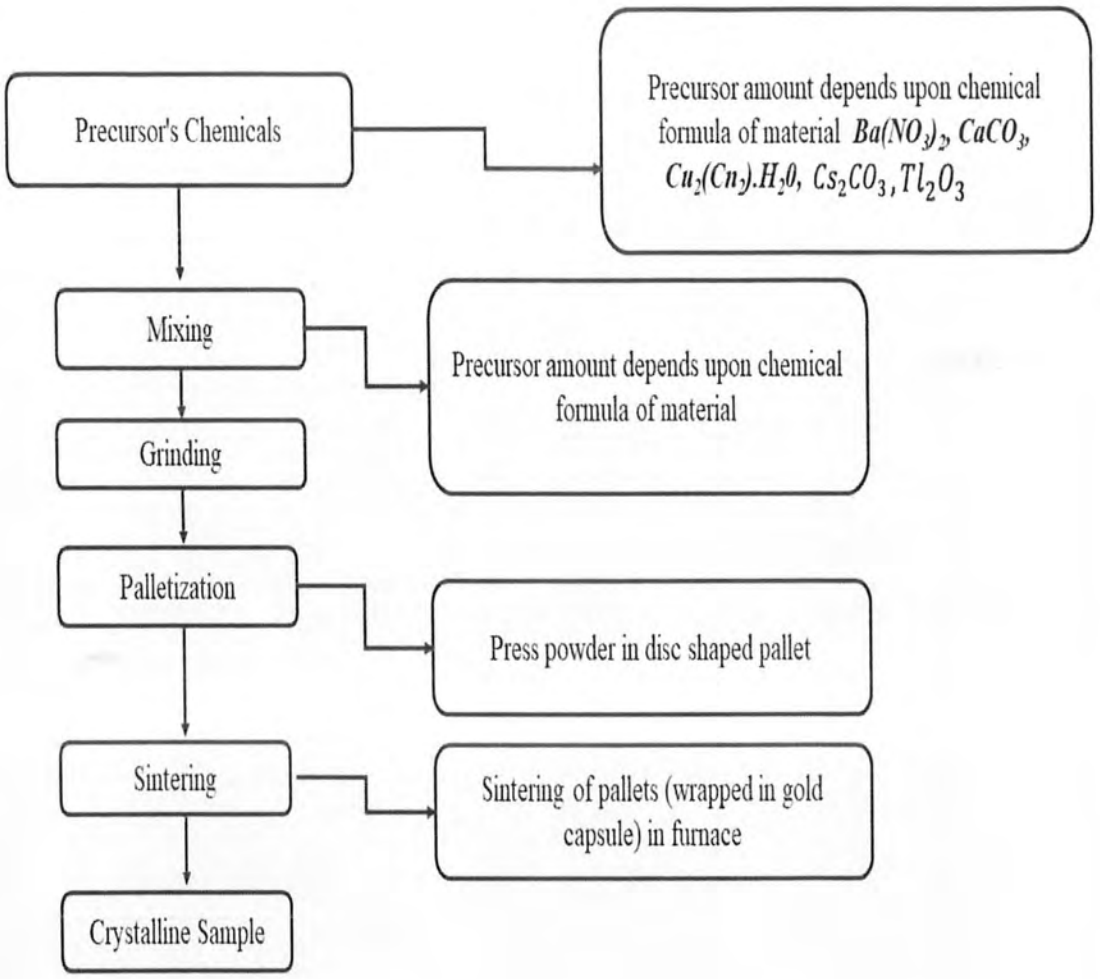

Figure 3-1:Different Steps for Preparation of Bulk Material

3.2 Characterization techniques

The schematic diagram for the techniques used for characterization of our superconducting samples is shown is below.

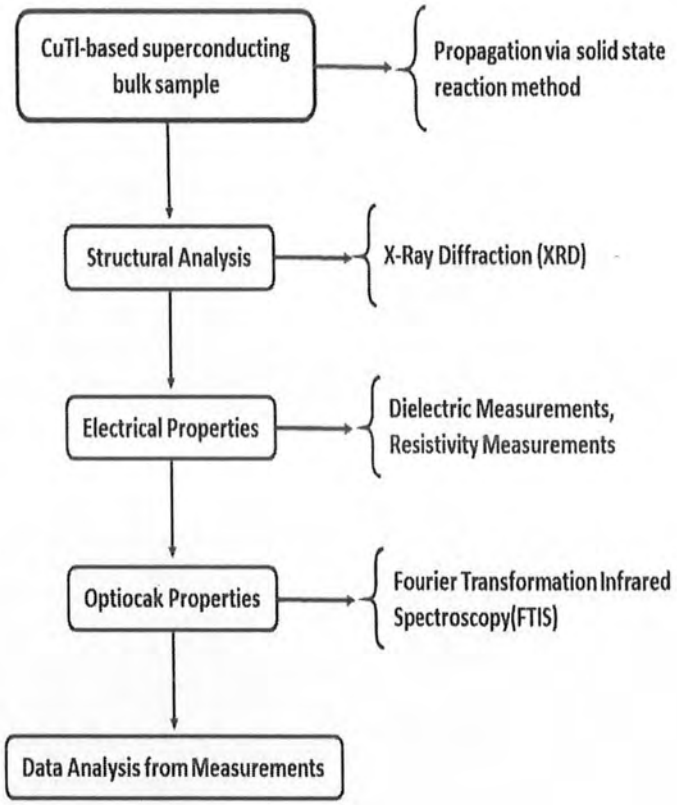

Figure 3-2: Schematic of Experimental Techniques

3.3 Characterization

In this section we are able to discuss experimental in addition to theoretical strategies for the characterization of samples. The prepared samples are characterized by means of the following strategies.

- A X-Ray Diffraction.
- A Resistivity Measurement.
- A Fourier Transform Infrared Spectroscopy.
- Fluctuation induced conductivity analysis.
- Dielectric measurements.

3.3.1 X-Ray diffraction

The technique of X-ray diffraction is used to determine the material's structure, i.e. whether it is crystalline or amorphous. The technique provides the information about different phases, and parameters of the unit cell of crystalline material. This technique uses the phenomena of diffraction which imposes the condition that the spacing between the atom should be comparable to the wavelength of X rays. Usually Cu or Mo are used to produce X-rays having wavelength 1.54Å and 0.8Å, respectively [1-2]. Bragg was the first scientist who proposed the diffraction of X-rays through crystalline material [3]. In the crystal the atom arranged in a regular manner having interatomic spacing comparable to the wavelength of the wave which subsequently act as a perfect 3-dimensional diffraction grating. The diffraction of x rays through the first three planes is as shown in figure 3-3.The path difference between two parallel planes is given as

$$\text{Path difference} = AB + BC \qquad (3.1)$$

$$\text{here} \quad AB = BC = dSin\theta \qquad (3.2)$$

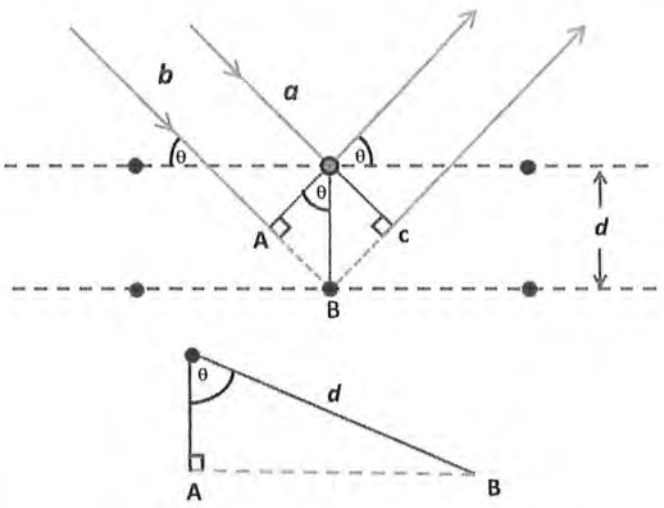

Figure 3-3:Schematic Diagram of a X-ray Diffraction Through Crystal

The path difference must be the integral multiple of the wavelength for the constructive interference.

$$\text{Path difference} = 2d\sin\theta = n\lambda \qquad (3.3)$$

Here n is a positive integer, d is interplanar spacing, θ is diffracted angle, and λ is the wavelength of X-rays.

For structural analysis of our samples we used D8 Focus, Bruker model XRD machine. The x-ray source used is Cu with kα lines having wavelength of 1.5406 Å. The range of '2θ' selected is from 4 to 60°. The scan speed was 0.8 sec/step. The diffraction data is collected on a computer system. To extract the structural information of samples from XRD data we use a computer program 'check cell'. The cell parameters 'a', 'b' and 'c' determined using check cell software. The unit cell volume for each sample was calculated using the values of the cell parameters. By putting the values of cell parameters in check cell software the corresponding miller indices (hkl) are calculated. Finally, the XRD graphs and all its corresponding parameters are designed in origin software.

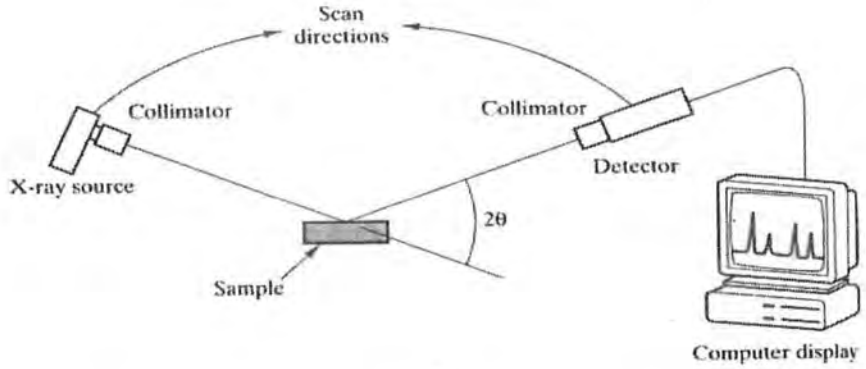

Figure 3-4:The schematic Diagram of the X-ray Diffractometer

3.3.2 Electrical Resistivity Measurements

As the conductor have free electron, which can move freely in all direction. But by the application of applied voltage all the electron moves in the same direction establish a current across the conductor. The lattice/phonon and defects in a conductor hinder the flow of electron that give rise to a resistance (R) in a conductor which can be calculated by using Ohm's law i.e.

$$V = IR \qquad (3.4)$$

Here, "I" represents the current that is passing through the conductor. "V" stands for the voltage applied across the conductor's ends, while "R" stands for the conductor's resistance.

A conductor's resistance is directly proportional to its length "L" and inversely proportional to its cross-sectional area "A". i.e.

$$R = \rho \frac{L}{A} \qquad (3.5)$$

Here 'ρ' is the function of temperature and it is named as the resistivity of the conductor. So

$$R(T) = \rho(T)\frac{L}{A} \qquad (3.6)$$

$$\rho(T) = R(T)\frac{A}{L} \qquad (3.7)$$

But from the Ohm's law

$$R(T) = \frac{V}{I}$$

So now we get the equation (3.7) as,

$$\rho(T) = \frac{V}{I}\frac{A}{L}$$

$$\rho(T) = \frac{VA}{IL} \qquad (3.8)$$

Here we measure area in cm^2, length in cm, current in amperes and voltage in volts such that the unit of the resistivity becomes 'Ω-cm'.

3.3.2.1 Four probe method for resistivity measurements

In two-probe resistivity, we can measure the resistivity up to Ω-m. However, in four-probe method we can measure the resistivity up to mΩ-m or micro ohm-meter. Typically, this technique is used to evaluate the resistivity of semiconductors, superconductors, metals, and polymers.

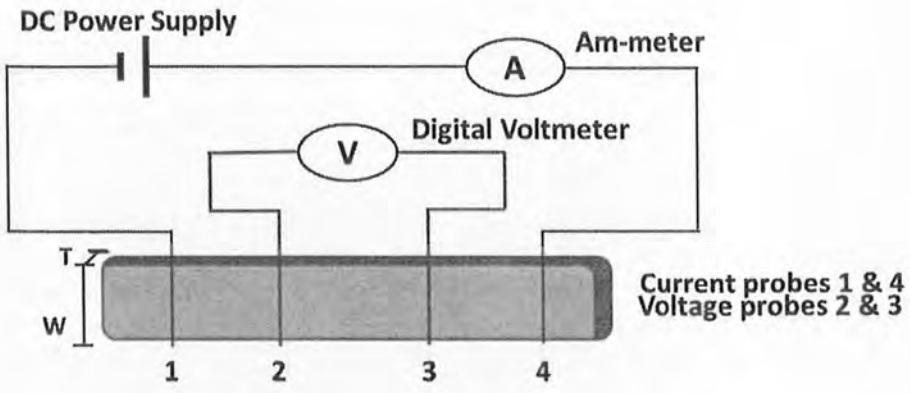

Figure 3-5: Diagram Exhibiting four-probe Method's Setup

Figure 3-5 illustrate the experimental configuration of Four Probe Resistivity Measurement method. With the help of silver paste, four contacts are secured to the sample's surface in this approach so that they won't break when the sample is cooled to a very low temperature. A outer wires maintain the 'current while the inner wire manifest drop in voltage across the sample. This voltage drops reported due to the resistance of the sample. We preferred for-probe method over two-probe method because as the contact resistance has a significant effect on overall resistance of the sample. So, with the help of four probe method we exclude the contact resistance and measure only the resistance across the sample [4].

If "V" is the voltage drop across the sample and "A" is the cross-sectional area through which the current "I" flows through the sample, the resistivity of the sample is then define as.

$$\rho(T) = V(T)A/IL \qquad (3.9)$$

Here V(T) is temperature dependent variable and L is the distance between inner voltage wires.

3.3.3 Fourier transform infrared spectroscopy

The vibrations of atoms occur about equilibrium position in solid. These vibrations/phonons have direct dependence upon the mass of atoms, their bond lengths with other atoms and bond angle. These dependencies brought changes in vibrations in different solid materials. Additionally, these vibrations are present at absolute zero. By using a quantum mechanical approach to simple harmonics, the energies associated with these lattice vibrations are.

$$E_n = \left(n + \frac{1}{2}\right)\hbar\omega_o \quad for \quad n = 0, 1, 2, 3 .... \qquad (3.10)$$

Here ħ is Boltzmann constant and have value, ħ = h/2π ~$1.054 \times 10^{-34}\, J.s$ and so "ω_o" here is a frequency of a harmonic oscillator. For n=0 the ground state energy, also these vibrations have energy $E_0 = \frac{1}{2}\hbar\omega_o$. For explanation of the physical properties of the sample these vibrations of lattice are most important. Hence, for the explanation of the characterization of a solid materials, so it is essential to find out what kind of vibrational modes are present in a sample. For studying these modes, we use a spectrometer known as Fourier transform infrared (FTIR) radiation spectrometer. This technique is known as FTIR spectroscopy.

FTIR has three main components: 1) a radiation source, 2) a Michelson interferometer, and 3) a detector.Michelson interferometer consists of three active components: i) a movable mirror, ii) a fixed mirror, and iii) a beam splitter and Two mirrors are placed perpendicular to each other as shown in figure 3.6. A beam splitter is a semi-reflective device, typically fabricated by depositing a thin layer of a germanium on a KBr substrate. Radiations from the source are generated toward the interferometer and fall on the beam splitter which reflected half of the radiations toward the fixed mirror while half of the radiations are transmitted toward the moving mirror. These two mirrors reflect the radiations which're then recombined at the beam splitter. The two reflected radiation beams interfere, and the resulted beam is called interferogram. The interferogram is then passed through the sample which absorb or transmit these radiations depending on the nature of the sample. A final interferogram is obtained on a detector. Each point of interferogram consists of all the frequencies of the source radiation. But for the analysis we required a single intensity value for each frequency value. So, we cannot analyse the measured interferogram directly. Therefore, a mathematical tool called Fourier transform is used to obtain a single frequency value for each absorption value. This is a reason why this technique is called Fourier transform infrared spectroscopy [5].

FTIR can be used for the following purposes.

- Identification of unknown materials
- Determination of quality of a material
- Determination of amount of different components in a material

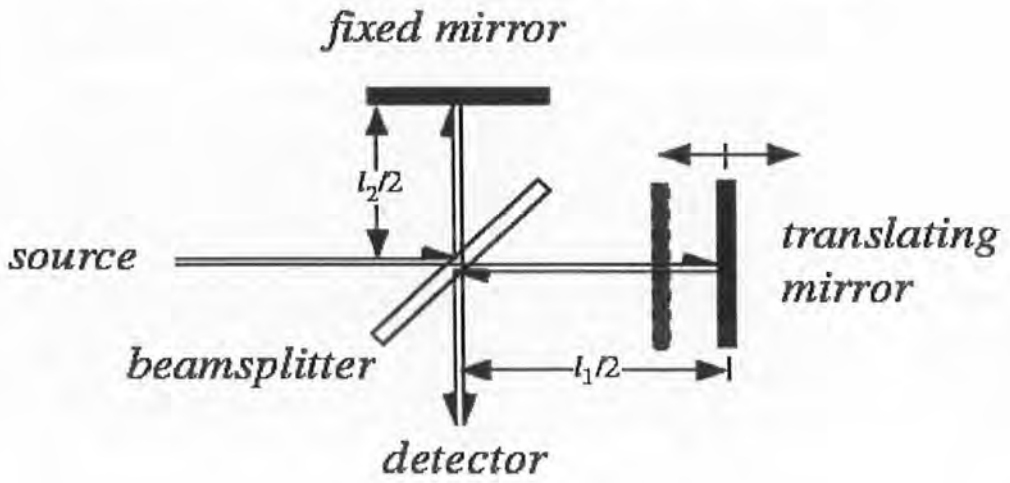

Figure 3-6:Schematic Diagram of Michelson Interferometer

We used a Nicolet 5700 model spectrometer in our experimental setup. For the background spectrum we used KBr in the form of thin pellet. After collecting a background spectrum, a small amount of sample is mixed with KBr powder and pelletized at 3.8 tons/cm2 of pressure. The pellet is then placed in a sample holder of spectrometer. The wavenumber range is set as 400 – 700 cm^{-1} and 200 scans was taken for each sample. The raw data is studied using a computer software Omnic. Different vibrational modes are observed for each sample and finally we compare vibrational modes of all samples.

3.3.3.1 Experimental method of FTIR

The experimental procedure to study the vibrational modes of sample is as follows: In the first step KBr pallets are used as background reference pallets. Then we add small amount of particles of our superconducting sample in KBr which is mixed for 5-10 minutes. These pallets are then placed in a sample holder for absoption spectrum. Using KBr spectrum as background we subtract it and get the spectrum of our superconducting material. Finally the software OMNIC is used to analyze the vibrational modes of our material.

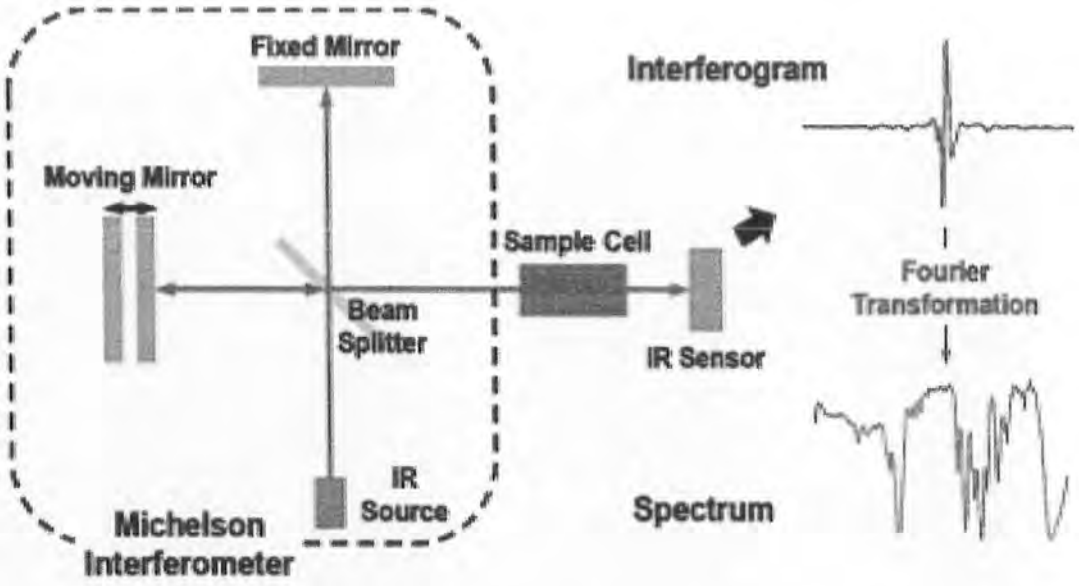

Figure 3-7: Optical Layout of FTIR Spectrometry

3.3.4 A Fluctuation Induced Conductivity (FIC) analysis

A Fluctuation induced conductivity analysis also known as para conductivity analysis is an approach to study fluctuations in superconductor, this results from the formation and annihilation of Cooper pairs down to the onset temperature. Cooper pairs start to form above transition temperature but due to thermal fluctuation these pairs continuously create and annihilate till $T_c(R=0)$. There creation and annihilation give rise to fluctuations in superconductor. The density of fluctuation decreases as we cooled our sample below Tc(R=0) where thermodynamic fluctuation cannot play an effective role to destroy the formation of cooper pair. Consequently, condensation of cooper pairs occurred give rise to zero resistance [6]. These fluctuations that induced conductivity exhibit for a temperature regime near Tc known as Ginzburg criterion temperature (T_G). For low temperature superconductors the value of T_G is less than 1 μK whereas it is around 1 – 2 K for the HTSCs. Therefore, it is possible to analyse these fluctuations. Ginzburg was the first scientist who probe the contribution of fluctuations to heat capacity and formulate the value of temperature where fluctuation modification to heat capacity is important as determine by relation below.

$$\frac{\Delta T}{T_c} \sim \left[\frac{(T_c)^4}{\varepsilon_f}\right] \sim \left[\frac{(a)^4}{\xi}\right] \sim 10^{-4} \; to \; 10^{-16} \qquad (3.11)$$

Here 'ξ' represents coherence length and 'a' represent inter-atomic separation between two lattice sites. The value of $\Delta T/T_c$ is so small therefore these fluctuations were undetectable experimentally for a long time.

Due to the variation that caused conductivity to deviate noticeably from its linear dependency at higher temperatures, given as.

$$\Delta\sigma(T) = \frac{\rho_N(T)-\rho(T)}{\rho_N(T)\rho(T} \qquad (3.12)$$

Here the ρ(T) denotes the actual resistivity and a $\rho N(T) = \alpha + \beta T$ represent a normal state extrapolated resistivity.Two distinct types of a fluctuation are typically regarded as (T). The first is the Aslamazov-Larkin (AL) contribution, which is linked to excess current that develops as a result of Cooper pair oscillations at temperatures higher than Tc [7-8]. The second one, a Maki-Thompson (MT) contribution, discussed how superconducting carrier fluctuations affected the

conductivity of ordinary electrons. The crossover point between a three-dimensional (3D) electronic state and a two-dimensional (2D) electronic state is shown by a different model called the Lawrence-Doniach (LD) model. The 'MT' term has a dependence on phase-relaxation time 't_φ' and exhibits a large effect in the 2D fluctuation area for moderate pair breaking, whereas the 'AL' term is found close to 'Tc'. Hence, the FIC offers insightful data regarding the superconductor's dimensionality, phase relaxation time t_φ, and coherence length $\xi_c(T)$. The analysis of crossover temperatures by using LD model have been testified by various researchers but here the MT contribution didn't convince many researchers because of their lacking possibility to evaluate τ_φ.

FIC analysis of polycrystalline bulk material is mainly consistent with the characteristic of 3D fluctuation, but the results are bit different from thin films and here 3D to 2D crossover has been observed in thin films with strong c-axis orientation.. The superiority of 3D fluctuations or 2D-3D crossover is temperature dependent.. Different experimental results have been discovered in the case of a single crystal[9].

3.3.5 Dielectric measurements

Dielectric properties determine the way a material reacts to the external electric field. The external electric field shifts the charge from its equilibrium position, leading to the development of polarization. Depending on the frequency of external electric field, there are four types of polarization [10].

- A Electronic polarization: It appears as a result of the shifting of atom and ion electronic charge clouds. This happens quite frequently at a frequency (10^{15}Hz)
- Atomic polarization: This polarisation is caused by the displacement of the ion core and the electronic charge distribution combined. These polarizations operate in the (10^{10}-10^{13} Hz) frequency band.
- A dipolar polarization: It originates from permanent dipoles which is activated at lower frequencies ($10^3 - 10^6$ Hz)
- Interfacial polarization: This involves limited movement of charge dipoles under applied field and are sensitive to low frequency range of 100 to few kilo Hertz
- The dipolar and interfacial polarization are important in our case because of their low frequency range. At high frequency the superconducting samples can be turned into normal materials [11-12].

For taking dielectric measurements of our sample we paste silver on both side of our sample to make it a capacitor. The silver paste behaves like a plate having dielectric medium (sample) between them. We use a Wayne Kerr 4275 LCR metre in a frequency range of 20 Hz to 1 MHz to measure the capacitance and conductance of our samples. From these capacitance (C) and conductance (G) values, we calculated the values of dielectric constants (ε', ε''), ac-conductivity (σac).

3.4 References

[1] B.D. Cullity, Elements of DIFFRACTION, 2nd Edit, Addision-Wesely Publishing Company, Inc. London, (1977).

[2] M.A. Omer, Elementary Solid State Physics, First Edit, Wesely Publishing Company (1974).

[3] Thomsen, John S, A. F. Burr, American J Phy 36.9 (1968) 803-810

[4] N.W.A. and N.D. Mermin, Solid State Physics, World Publishing Corporation, (1976).

[5] Introduction to Fourier Transform Infrared Spectroscopy, Thermo Nicolet Corporation (USA), (2001).

[6] M.A.R. · S.A. · N.H. · N.A.K. Khan, J Supercond Nov Magn 27.11 (2014) 2427–2434.

[7] L.G.A. and A.L. Larkin, Phy.Lett. A 26 (1968) 238–339.

[8] M. Muzaffar, M. Usman, N. A. Khan, Int J Mod Phys B 30.18 (2016) 1650112.

[9] S.J. Hagen, Z.Z. Wang, N.P. Ong, Phys. Rev. B 37.13 (1988) 7928

[10] A. Younis, N.A. Khan, Mod. Phys. Lett. B 24 (2010) 3097–3107.

[11] Ş. Çavdar, H. Koralay, N. Tuğluoğlu, A. Günen, Supercond. Sci. Technol. 18 (2005) 1204–1209.

[12] N.A. Khan, A. Saba, A. Raza, J. Alloys Compd. 757 (2018) 476–483.

CHAPTER-04
4 RESULT AND DISCUSSION

4.1 Introduction

The $Cu_{0.5}Tl_{0.5}Ba_2Ca_2Cu_3O_{10-\delta}$ superconductor has a charge reservoir layer made of $Cu_{0.5}Tl_{0.5}Ba_2O_{4-\delta}$ and four conducting CuO_2 planes. Due to its higher Fermi level, the charge reservoir layer supplies the carriers to the conducting CuO_2 planes, and these conducting planes exhibit superconductivity. The thickness of the charge reservoir layer is critical in determining carrier density in the conducting CuO_2 planes. The density of carriers in these planes determines the shape of the Fermi-surface and its instability around the Fermi-level, which would eventually develop density of Cooper-pairs in the superconducting state. The charge reservoir layer thickness would turn conducting CuO_2 planes with carrier density in over-doped, under-doped, or optimally doped regimes, determining the final critical temperature of the superconducting compound[1-8].The maximum critical temperature is observed in the ideally doped compounds, where the hole density is approximately 0.4 holes/CuO2 planes, and the charge density in the CuO_2 versus critical temperature of the superconducting compounds follows a bell-shaped phase diagram.$Cu_{0.5}Tl_{0.5}Ba_2Ca_2(Cu_{3-x}Cs_x)O_{10-\delta}$(x=0.5,1,1.5,2,2.5,3) samples were synthesised to examine the role of the charge reservoir layer thickness in present investigations. The $Cu_{0.5}Tl_{0.5}Ba_2O_{4-\delta}$ charge reservoir layer is fixed in the second portion of these research, but the CuO_2 planes are doped with Cs atoms, which would directly increase the density of free electrons in the conducting planes. Alkali metals are well-known s-electron donors. We created Cs-doped $Cu_{0.5}Tl_{0.5}Ba_2Ca_2(Cu_{3-x}Cs_x)O_{10-\delta}$ (x=0.5,1,1.5,2,2.5,3) samples and investigated their role in the mechanism of high 'Tc' superconductivity. Previous research has shown that doping smaller sized 'Mg' atoms at the 'Ca' sites improves inter-plane coupling, which has also been studied for such compounds[9].

When exposed to external electric fields, solid state media such as $Cu_{0.5}Tl_{0.5}Ba_2Ca_2(Cu_{3-x}Cs_x)O_{10-\delta}$(x=0.5,1,1.5,2,2.5,3) samples become polarised. Various polarisation mechanisms emerge in such materials depending on the strength of the applied electric frequency, such as:

- ❖ Electronic polarisation (ε_e) is typically observed at extremely high frequencies of the order of 10^{15} Hz (i.e. in ultraviolet optical range)
- ❖ In the infrared frequency range (10^{10} to 10^{13} Hz), atomic and ionic polarisation (ε_a) is observed.
- ❖ The observed dipolar or oriental polarisation is (ε_o) in the sub-infrared frequency range (10^3 to 10^6 Hz).
- ❖ Interfacial polarisation (ε_i) is typically sensitive at low frequencies (10^2 Hz) and can extend to a few kilohertz, which primarily contributes to the dielectric properties of the materials in our case.

The active interfacial and dipolar polarisation (i.e. 40-3000Hz) is of primary interest to us because material remains superconducting at such low frequencies.

4.2 Experimental:

$Cu_{0.5}Tl_{0.5}Ba_2Ca_2(Cu_{3-x}Cs_x)O_{10-\delta}$ (x=0.5,1,1.5,2,2.5,3)sample. $Ca(NO_3)_24H_2O$, $Ba(NO_3)_2$, $CsCO_3$, and $Cu_2(CN)_2+H_2O$, were used as starting materials. In the first stage, these compounds are mixed according to the desired composition with an agate pestle for approximately one hour. The well-mixed material is fired twice at 860°C for 24 hours in a chamber furnace in a quartz boat, heat-treated in the furnace, and then cooled to room temperature. Repeating the process in an alumina boat and cooling the material each time to room temperature following the heat treatment results in a material of high grade. The second and last stage involves mixing the treated precursor material for roughly an hour with the predicted amount of Tl_2O_3 to produce samples of $Cu_{0.5}Tl_{0.5}Ba_2Ca_2(Cu_{3-x}Cs_x)O_{10-\delta}$(x=0,0.5,1,1.5,2,2.5,3)as the final reactants compositions. Thallium oxide-mixed material is compressed by a hydraulic press to 3.8 tons/cm2 pressure, forming pellets that are then enclosed in gold capsules. Pellets containing gold are heated for 10 minutes at 860°C in a chamber furnace. The obtained samples are characterized by X-ray diffraction (XRD), temperature dependent resistance measurements, FTIR absorption spectroscopy, and dielectric measurements. X-ray diffraction was performed on a Bruker DX 8 Focus using CuKα radiation with a wavelength of 1.54056 Å and cell parameters were determined by the check Cell Refinement computer program. Temperature-dependent resistivity

measurements of materials are performed using the four-probe method. Using NICOLET 5700 and KBr as a background material,FTIR absorption measurements were made in the 400–700 cm^{-1} wavenumber region. On a Wayne Kerr 4275 LCR Meter, frequency dependent dielectric measurements are made in the frequency range of 20-3000Hz using the two-probe method. Measurements were carried out at a constant temperature of 80K while the contacts on the sample's surface were formed with silver paste. Conductance (G) and capacitance (C) of samples are measured in dielectric measurements. The following formulas are used to compute the samples' dielectric constant (ε_r), dielectric loss ($\tan\delta$), and ac-conductivity (σ_{ac}) from conductance (G) and capacitance (C)[10].

$$\varepsilon_r = \varepsilon_m / \varepsilon_0 \qquad (4.1)$$

'ε_m' is a permittivity of a material, 'ε_0' is a permittivity of a free space, and 'ε_r' is a relative permittivity

$$\varepsilon' = Cd/A\varepsilon_O \qquad (4.2)$$

so here 'C' is the capacitance of the pellet (F), 'd' is a thickness of the pellet (m), 'ε_0' is a permittivity of a free space ($\varepsilon_0 = 8.85 \times 10{-}12$ F m−1) and 'A' is the area of the electrode (m^2).

$$\varepsilon'' = Gd/A\varepsilon_0\omega \qquad (4.3)$$

here, angular frequency ($\omega=2\pi f$) is used. The formula for dielectric loss tan δ is expressed as.

$$\tan\delta=\varepsilon''/\varepsilon' \qquad (4.4)$$

The alternating current (ac) conductivity σac is written as.

$$\sigma_{ac}= 2\pi f\varepsilon_0\varepsilon'\tan\delta \qquad (4.5)$$

here f is the frequency of the applied ac field (Hz).

4.3 Inferences and Discourse:

4.3.1 Investigation of x-ray scans

Figures 4-1 and 4-2 shows X-ray diffraction scans of $Cu_{0.5}Tl_{0.5}Ba_2Ca_2(Cu_{3-x}Cs_x)O_{10-\delta}$ (x=0.5,1,1.5,2,2.5,3) samples.

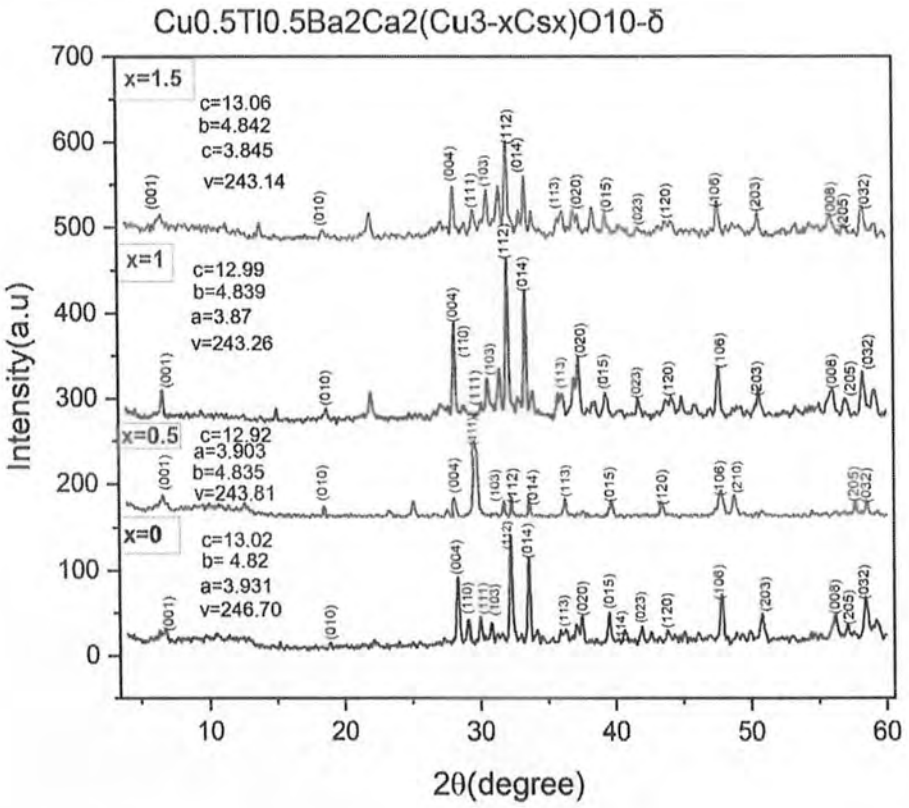

Figure 4-1: The XRD of $Cu_{0.5}Tl_{0.5}Ba_2Ca_2(Cu_{3-x}Cs_x)O_{10-\delta}$ (x=0,0.5,1,1.5) samples.

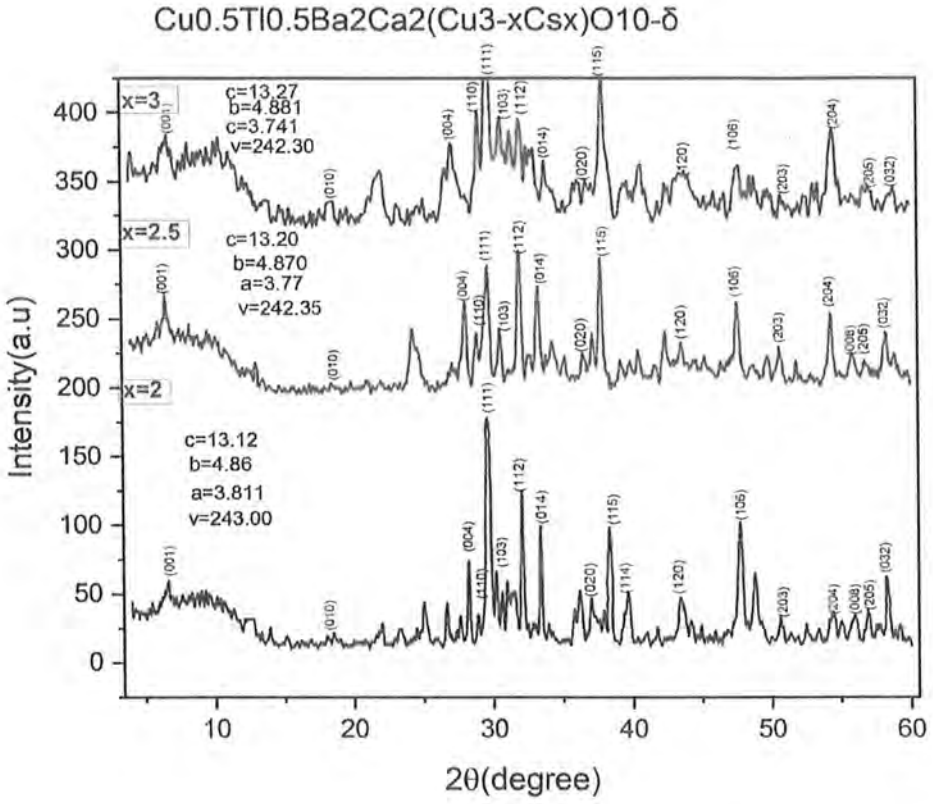

Figure 4-2:The XRD of a $Cu_{0.5}Tl_{0.5}Ba_2Ca_2(Cu_{3-x}Cs_x)O_{10-\delta}$ (x = 2,2.5,3) samples.

Under the PMMM space group all diffraction lines are fitted to the orthorhombic structure. The cell parameters are calculated using a computer programme called check cell.. Changes in c-axis length and unit cell volume versus doping concentration. The c-axis length (except for x=0.5 doping) increases slightly with increasing Cs doping, but its volume is suppressed with increasing Cs doping in the final compound.As shown in Fig 4-3, the suppression of the volume of the unit cell with increased Cs doping results in an increase in the density of carriers with enhanced Cs-doping in the final compound. As shown in Fig4-4, the a-axis length increases with increasing Cs doping level, while the b-axis length is suppressed, and their values are shown in Table (4.1).

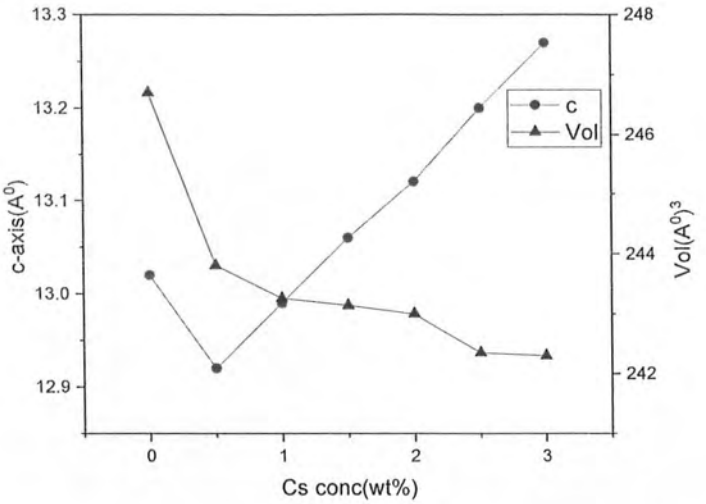

Figure 4-3: Comparison of C-axis and the volume of Cu0.5Tl0.5Ba2Ca2(Cu3-xCsx)O10-δ (x=0.5,1,1.5,2,2.5,3)Samples

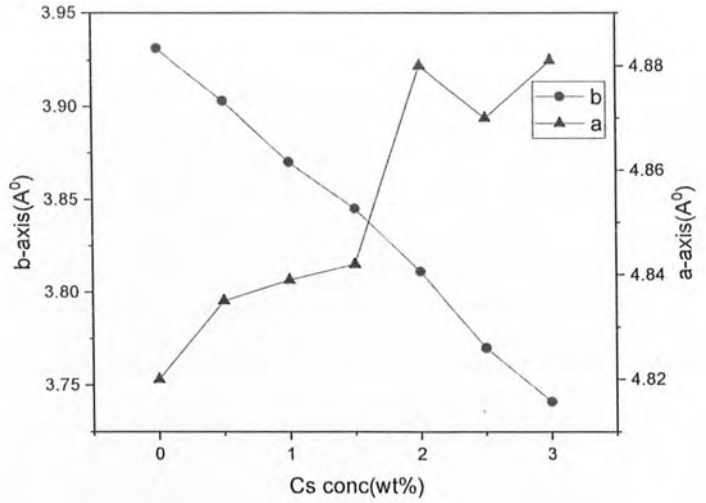

Figure 4-4:Comparison of a and b axis of $Cu_{0.5}Tl_{0.5}Ba_2Ca_2(Cu_{3-x}Cs_x)O_{10-\delta}$ (x=0.5,1,1.5,2,2.5,3)Samples

Cs conc. (wt%)	a-axis (A^0)	b-axis (A^0)	c-axis (A^0)	Volume $(A^0)^3$
0	3.931	4.82	13.02	246.70
0.5	3.903	4.835	12.92	243.81
1	3.87	4.839	12.99	243.26
1.5	3.845	4.842	13.06	243.14
2	3.811	4.86	13.12	243.00
2.5	3.77	4.870	13.20	242.35
3	3.741	4.881	13.27	242.30

Table 4-1: Lattice parameters of a $Cu_{0.5}Tl_{0.5}Ba_2Ca_2(Cu_{3-x}Cs_x)O_{10-\delta}$ (x=0.5,1,1.5,2,2.5,3) samples

4.3.2 Resistance Measurement

The measured resistivity versus temperature for the $Cu_{0.5}Tl_{0.5}Ba_2Ca_2(Cu_{3-x}Cs_x)O_{10-\delta}$ (x=0.5,1.1,5,2,2.5,3) samples are shown in Fig4.5. In Fig. 4-6, all of these samples exhibit metallic variations in resistivity from room temperature to 77 K, with the onset of superconductivity occurring at 107.9, 106.6, 107.1, 104.5, 109.2,112.8 and 120.8 K, respectively, and the zero resistivity critical temperature occurring at 91.9, 95.7, 88.9, 94.2, 91.2, 90.3, and 95.3 K and their values are given in table 4-2.

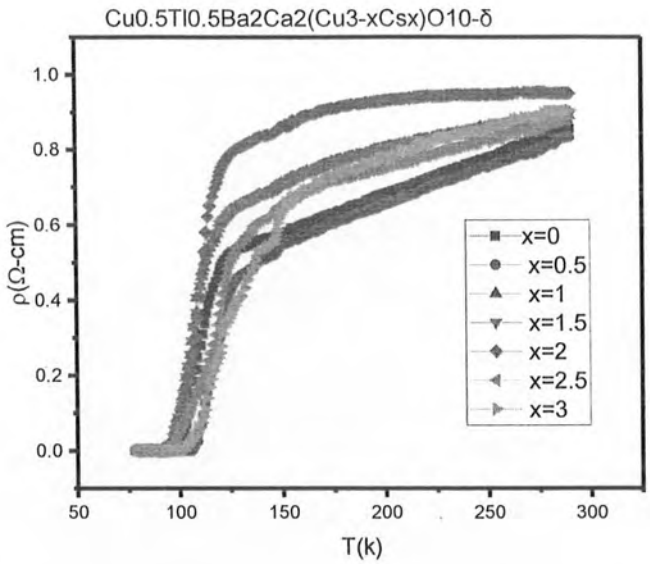

Figure 4-5:Resistivity vs Temperature measurement of a $Cu_{0.5}Tl_{0.5}Ba_2Ca_2(Cu_{3-x}Cs_x)O_{10-\delta}$ (x =0.5,1,1.5,2,2.5,3) samples

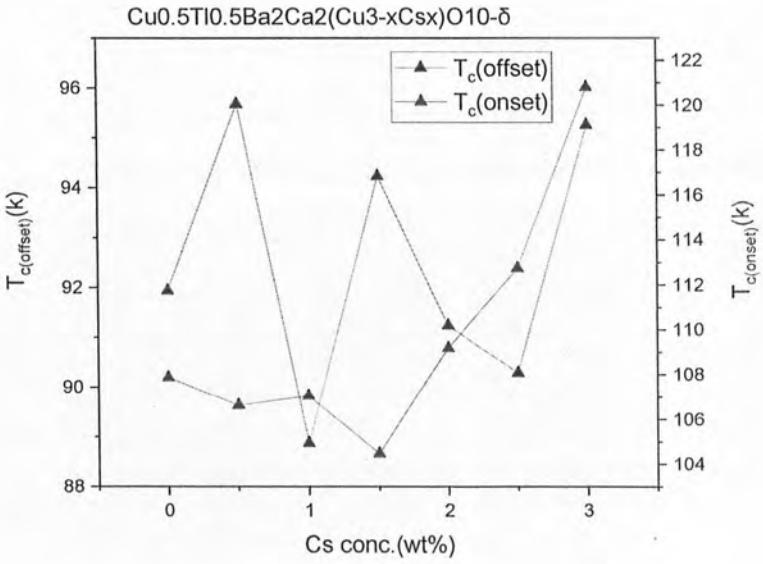

Figure 4-6: Variation of T_c(onset) and T_c(R=0) by Enhancing Cs-doping

Cs conc. (wt%)	T_c(R=0) (k)	T_c(onset) (k)
0	91.94	107.88
0.5	95.68	106.63
1	88.87	107.05
1.5	94.23	104.47
2	91.24	109.20
2.5	90.29	112.75
3	95.26	120.82

Table 4-2:Resistivity data of a $Cu_{0.5}Tl_{0.5}Ba_2Ca_2(Cu_{3-x}Cs_x)O_{10-\delta}$ (x=0.5,1,1.5,2,2.5,3)Samples

4.3.3 Fluctuation Induced Conductivity Analysis

The effects of trapped Cs atoms on the intrinsic superconducting parameters of $Cu_{0.5}Tl_{0.5}Ba_2Ca_2(Cu_{3-x}Cs_x)O_{10-\delta}$(x=0.5,1,1.5,2,2.5,3) samples were investigated by excess conductivity analysis.

The excess conductivity analyses of conductivity analyses of conductivity data is performed using the familiar Aslamazov Larkin equation which is given below.

$$\Delta\sigma_{(T)}=\Delta\sigma_{RT}\varepsilon^{-\lambda_D} \qquad (4.5)$$

So the above form of the equation can be written as.

$$\ln\Delta\sigma_{(T)}=\ln\Delta\sigma_{RT}-\lambda\ln(\varepsilon) \qquad (4.6)$$

so it is applicable in the temperature regime near 'T'.so here, $\varepsilon = \left[\frac{T-T_c^{mf}}{T_c^{mf}}\right]$ is a reduced temperature and 'λ_D' is a dimensional exponent. here the value of a dimensional exponent λ_D=0.3

corresponds to the critical regime, $\lambda_D = 0.5$ to the three dimensional conductivity regime(3D), $\lambda_D = 1$ to the two dimensional conductivities (2D) and $\lambda_D = 2.0$ zero dimension (0D) conductivities this arises from various thermal activation processes that occur during samples heating[11-12]. For polycrystalline samples, a modification of this equation by the Lawrence and Doniak (LD) model is proposed by

$$\Delta\sigma_{LD}=[e^2/(16\hbar d)](1+Je^{-1})^{-1/2}\,\varepsilon^{-1} \qquad (4.7)$$

where $J= [2\xi_{c(0)}/d]^2$ is the inter-CuO_2-layers couplings, the 'd' is a thickness of superconducting layers ~18Å for CuTl-1234 samples) and the $\xi_{c(0)}$ is the coherence length along the c-axis. The coherence length is calculated using the LD model's crossover temperatures of three-dimensional exponents of two-dimensional conductivities:

$$\xi_{c(0)} = d/2[(T_{3D\text{-}2D}/ T_{mf})-1]^{1/2} \qquad (4.8)$$

The Cooper-phase pair's relaxation time is calculated using the following equation:

$$\tau_\phi = \frac{\pi\hbar}{8k_B T\varepsilon_0} \qquad (4.9)$$

The following expression is used to calculate the coupling constant J:

$$J = \frac{\hbar\tau_\phi^{-1}}{2\pi k_B T} \qquad (4.10)$$

The Fermi velocity of a charge carrier and the energy required to destroy a Cooper pair are:

$$V_F = \frac{5\pi k_B T_c \xi_{c(0)}}{2K\hbar} \qquad (4.11)$$

$$E = \frac{h}{\tau_\phi(1.6\times10^{-19})}\,(\text{eV}) \qquad (4.12)$$

In the expression above, K≡0.12[13] is used as a value. Table4-3 provides the cross over temperatures that arise from a log plot of the excess conductivity versus the lowered temperature.

Samples	λ_{CR}	λ_{3D}	λ_{2D}	λ_{0D}	$T_{CR-3D}=T_G$ (K)	T_{3D-2D} (K)	T_{2D-0D} (K)	T_c^m(K)	T^* (K)	$\alpha=\rho_n(0K)$ (Ω-cm)
0	0.32	0.56	1.06	1.93	106.9	106.5	107.3	103.4	126.4	0.029
0.5	-	0.5	1.12	2.05	105.3	105.4	104.1	94.2	124.2	0.035
1	-	0.51	1.07	2.16	102.4	103.2	101.6	95.8	118.5	0.041
1.5	0.31	0.53	1.05	1.98	100.3	100.9	99.4	96.1	111.3	0.053
2	-	0.54	1.03	1.91	99.5	98.3	97.9	96.8	109.3	0.061
2.5	-	0.54	1.033	1.88	97.1	96.5	96.3	97.1	117.7	0.072
3	-	0.5	1.039	1.85	96.4	95.2	94.1	98.3	121.6	0.081

Table 4-3: Parameters Estimated From diagram of $\ln(\Delta\sigma)$ vs $\ln(\varepsilon)$

These temperatures shift to lower values with increasing Cs doping of the sample.So the Important superconductivity parameters of a $Cu_{0.5}Tl_{0.5}Ba_2Ca_2(Cu_{3-x}Cs_x)O_{10-\delta}$ (x=0,0.5,1,1.5,2,2.5,3)samples include $\xi c(0)$, the inter-layer coupling J and V_F (the Fermi velocity) and the phase relaxation time of the superconducting carriers are displayed in Table 4-4.

Sample	$\xi_c(0)$ (Å)	J	N_G	$\lambda_{p,d}x10^2$ (Å)	$B_{c(0)}$ (T)	$B_{c1(0)}$ (T)	$B_{c2(0)}$ (T)	κ	$J_{c(0)}x10^3$ (A/cm^2)	V_Fx10^7 (m/s)	E_{Break} (eV)	τ_φ x 10^{-13} (s)
0	1.99	0.071	0.047	6.8	2.06	0.14	126.2	47.7	1.67	1.74	0.04	1.8
0.5	2.10	0.075	0.048	7.01	2.01	0.09	126.2	48.1	1.59	1.81	0.01	3.9
1	2.15	0.08	0.049	7.2	1.98	0.085	126.2	48.9	1.48	1.89	0.015	3.7
1.5	2.19	0.083	0.051	7.9	1.75	0.079	126.2	51.1	1.3	1.9	0.018	3.5
2	2.22	0.089	0.052	8.09	1.63	0.069	126.2	51.8	1.15	1.97	0.02	3.1
2.5	2.28	0.09	0.052	8.15	1.59	0.063	126.2	53.4	1.01	2.01	0.027	2.9
3	2.35	0.092	0.054	8.22	1.55	0.059	126.2	54.5	0.93	2.15	0.03	2.7

Table 4-4: The Parameters estimated from excess conductivity analysis of $Cu_{1.5}Tl_{1.5}Ba_2Ca_2(Cu_{3-x}Cs_x)O_{10-\delta}$ (x=0.5,1,1.5,2,2.5,3) samples

These parameters have higher values in Cs-doped samples. Such parameters, which critically depend on the Fermi-vector via $K_F = [3\pi^2 N/V]^{1/2}$ (which depend on carrier density in this expression), show an increase in carrier density in the superconducting CuO2/CsO2 planes in Cs-doped samples.

The Ginzburg number 'N_G' is determined by the crossover temperature between the 3D LD regime and the Ginzburg Landau (GL), TG, regime:

$$N_G = \left| \frac{T_G - T_c}{T_c} \right| \qquad (4.13)$$

The following expressions are used to calculate important superconducting parameters using 'N_G' and a Ginzbur-Landau theory[14].

here $N_G = 1/2[K_B T_c / B_{c(0)}^2 \gamma^2 \xi_{c(0)}^3]^2$ (4.14)

and $B_{c(0)} = (K_B T_c / (2N_G)^{1/2} \gamma^2 \xi_{c(0)}^3)^{1/2}$ (4.14)

$$B_c = \frac{\Phi_0}{2\sqrt{2}\pi \lambda_{p.d(0)} \xi_{ab(0)}} \qquad (4.15)$$

$$B_{c1} = \frac{B_c}{\kappa\sqrt{2}} \ln \kappa \qquad (4.16)$$

$$B_{c2} = \sqrt{2}\kappa B_c \qquad (4.17)$$

$$J_c = \frac{4\kappa B_{c1}}{3\sqrt{3}\lambda_{p.d(0)} \ln \kappa} \qquad (4.18)$$

here $\gamma = \xi_{ab(0)}/\xi_{c(0)}$ is a superconductor anisotropy given by:

$$\gamma = \xi_{ab(0)}/\xi_{c(0)} = 5/(n-1) \qquad (4.19)$$

n=4 for a CuTl-1234 so the value of γ changes accordingly. $\kappa = \lambda/\xi$ [15] is a Ginzburg Landau (GL) parameter [ ] and T_c^{mf} is the mean critical magnetic field temperature determined from the temperature inflection point of the resistance derivative (dp/dT). The values of $B_{c(0)}$, $B_{c1(0)}$,

$B_{c2(0)}$, $J_{c(0)}$ and $\kappa=\lambda/\xi$ are calculated for $Cu_{0.5}Tl_{0.5}Ba_2Ca_2(Cu_{3-x}Cs_x)O_{10-\delta}$ (x=0.5,1,1.5,2,2.5,3) samples using the aforementioned equations and Ginzberg Landau number 'N_G', and their values are shown in table4-4. so the values of these parameetrs are increased in Cs doped $Cu_{0.5}Tl_{0.5}Ba_2Ca_2(Cu_{3-x}Cs_x)O_{10-\delta}$ (x=0.5,1,1.5,2,2.5,3) samples, indicating that the population of inadvertent local defects acting as a pinning centres is increased in doped samples consequently resulting into the enhancement of values of these parameters.

Figures 4-7, 4-8, 4-9, 4-10, 4-11, 4-12, and 4-13 show excess conductivity analyses of a $Cu_{0.5}Tl_{0.5}Ba_2Ca_2(Cu_{3-x}Cs_x)O_{10-\delta}$ (x=0.5,1,1.5,2,2.5,3) samples.

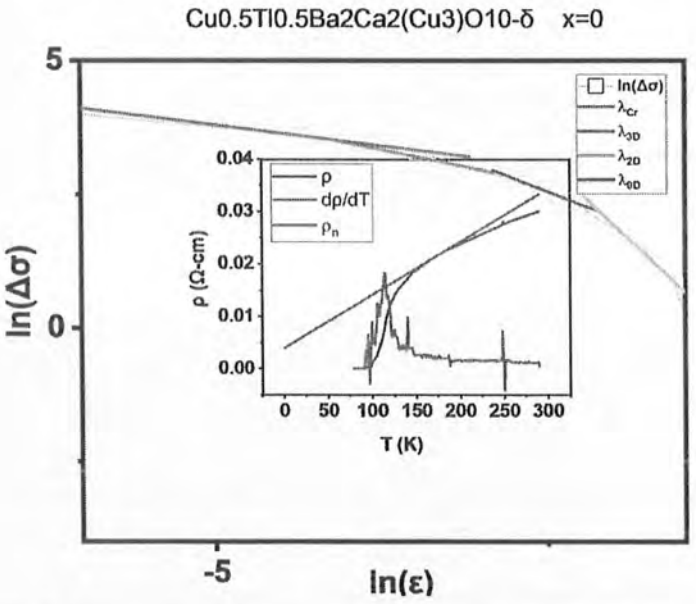

Figure 4-7: ln(ε) vs ln(Δσ) depiction of a $Cu_{0.5}Tl_{0.5}Ba_2Ca_2(Cu_3)O_{10-\delta}$ sample

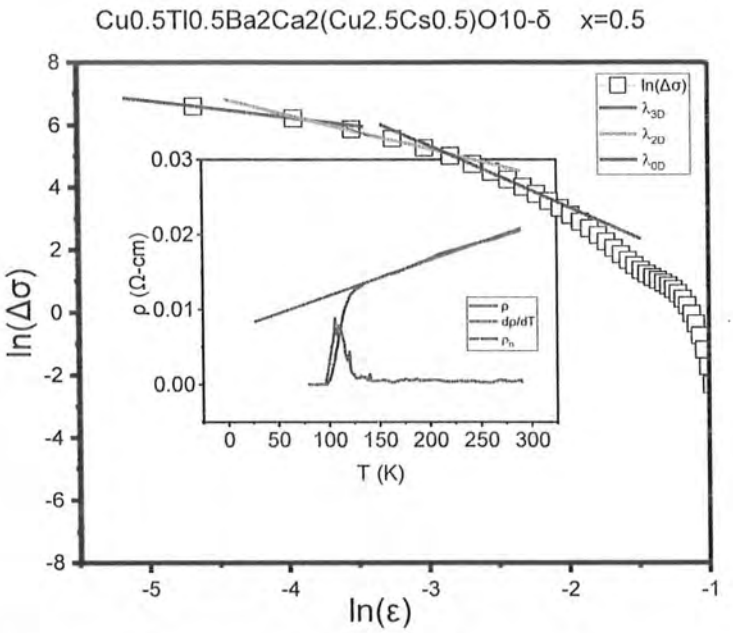

Figure 4-8:ln(ε) vs ln(Δσ) depiction of a $Cu_{0.5}Tl_{0.5}Ba_2Ca_2(Cu_{2.5}Cs_{0.5})O_{10-\delta}$ sample

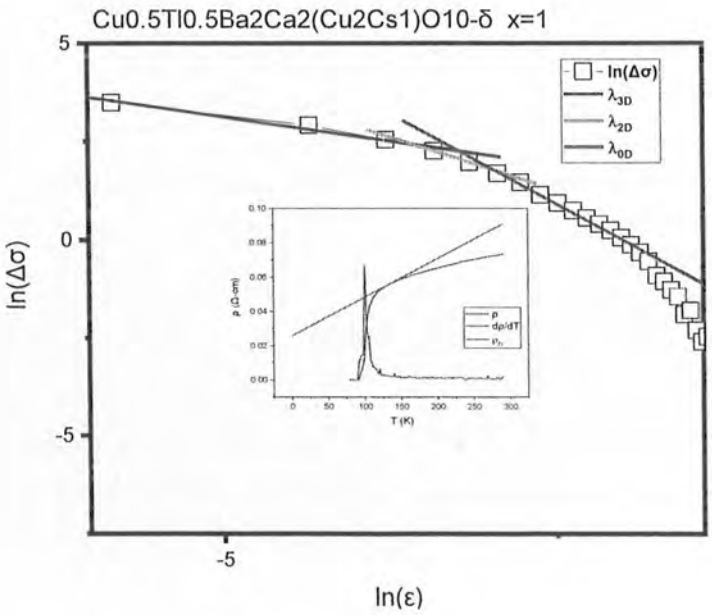

Figure 4-9:ln(ε) vs ln(Δσ) depiction of $Cu_{0.5}Tl_{0.5}Ba_2Ca_2(Cu_2Cs_1)O_{10-\delta}$ sample

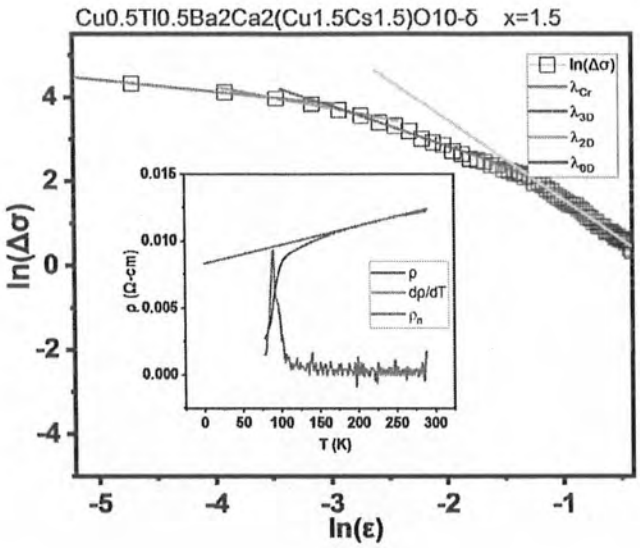

Figure 4-10:ln(ε) vs ln(Δσ) depiction of a $Cu_{0.5}Tl_{0.5}Ba_2Ca_2(Cu_{1.5}\ Cs_{1.5}\ )O_{10-\delta}$ sample

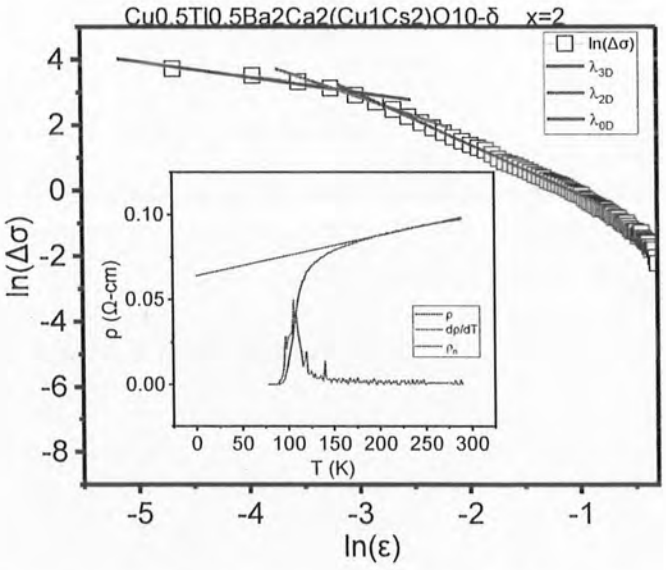

Figure 4-11:ln(ε) vs ln(Δσ) depiction of a $Cu_{0.5}Tl_{0.5}Ba_2Ca_2(Cu_1Cs_2)O_{10-\delta}$ sample

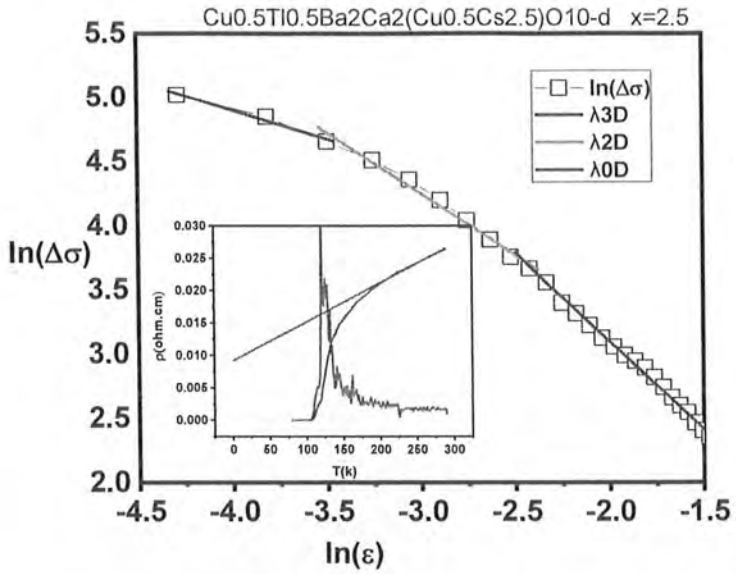

Figure 4-12:ln(ε) vs ln(Δσ) depiction of a $Cu_{0.5}Tl_{0.5}Ba_2Ca_2(Cu_{0.5}Cs_{2.5})O_{10-\delta}$ sample

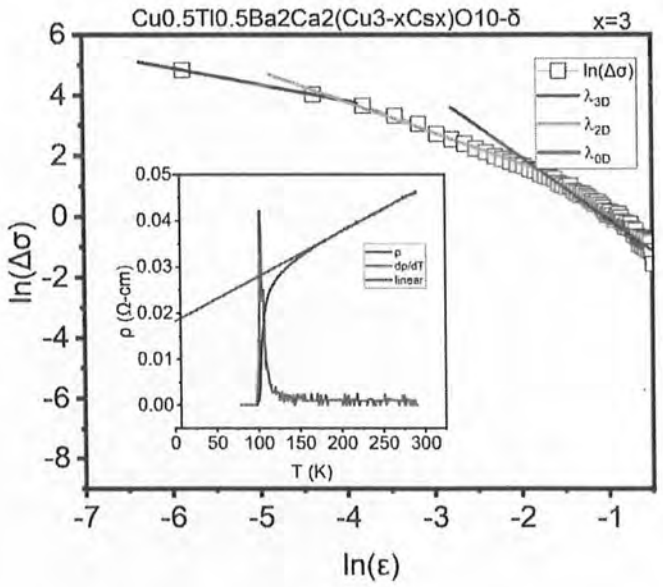

Figure 4-13:ln(ε) vs ln(Δσ) depiction of a $Cu_{0.5}Cl_{0.5}Ba_2Ca_2(Cs_3)O_{10-\delta}$ sample

Table4-3 shows various cross overs derived from the log plot of excess conductivity versus reduced temperature. Compared to $Cu_{0.5}Tl_{0.5}Ba_2Ca_2(Cu_{3-x}Cs_x)O_{10-\delta}$ (x=0.5,1,1.5,2,2.5,3) samples that are not doped T_G, T_{3D-2D} are shifted to the higher temperature values whereas the temperature T_{2D-0D} is shifted to low temperature values showing that more three dimensional characteristics are promoted in Cs-doped samples, Table3-4. Coherence length $\xi_{c(0)}$, along the c-axis, interlayer coupling J and V_F (Fermi velocity) of superconducting charges carriers, energy required to break the Cooper pair for $Cu_{0.5}Tl_{0.5}Ba_2Ca_2(Cu_{3-x}Cs_x)O_{10-\delta}$ (x=0.5,1,1.5,2,2.5,3) samples is suppressed compared to undoped $Cu_{0.5}Tl_{0.5}Ba_2Ca_3Cu_4O_{12-\delta}$, samples, and their values are in Table4-4.Using Ginzberg Landau number N_G the values $B_{c(0)}$, $B_{c1(0)}$, $B_{c2(0)}$, $J_c(0)$ and $\kappa=\lambda/\xi$ for a $Cu_{0.5}Tl_{0.5}Ba_2Ca_2(Cu_{3-x}Cs_x)O_{10-\delta}$ (x=0.5,1,1.5,2,2.5,3) are determined and their values are given in Table4-4.In a comparison to un-doped $Cu_{0.5}Tl_{0.5}Ba_2Ca_2(Cu_3)O_{10-\delta}$ samples, the values of these parameters are suppressed in doped $Cu_{0.5}Tl_{0.5}Ba_2Ca_2(Cu_{3-x}Cs_x)O_{10-\delta}$ (x=0.5,1,1.5,2,2.5,3) samples. The suppression of these parameters suggested that the population of inadvertent defects acting as pinning centres decreases in Cs-doped $Cu_{0.5}Tl_{0.5}Ba_2Ca_2(Cu_{3-x}Cs_x)O_{10-\delta}$ (x=0.5,1,1.5,2,2.5,3) samples compared to un-doped $Cu_{0.5}Tl_{0.5}Ba_2Ca_2(Cu_3)O_{10-\delta}$ samples. As a result, the energy required to break the Cooper pair increases in the Cs-doped sample, while the phase relaxation time of the charge carriers increases. Electrons are more tightly linked in Cs-doped samples, as evidenced by the rise in the energy needed to split Cooper pairs.

4.3.4 FTIR Analysis

FTIR absorbance readings for these samples are shown in Figure 4-14. Such superconductor samples exhibit three prominent absorption modes related to the vibrations of the oxygen atoms within the unit cell.Two of these are connected to the vibrations of apical oxygen atoms of the types Tl-O_A-Cu(2) around 450-480, Cu(1)-O_A-Cu(2) around 480-550 cm^{-1} and a CuO_2 planar oxygen mode around 570-590 cm^{-1}. In the Cs-doped samples,the apical oxygen mode of type Tl-O_A-Cu(2) form around 450-480 softens,while Cu(1)-O_A-Cu(2) around 480-550 cm^{-1} hardens. The planar oxygen modes around it are also softened in the Cs-doped sample, indicating that planar oxygen is attached to heavy Cs atoms with low oscillator strength in the unit cell. Moreover, these oxygen-related modes of softening and hardening also indicate the incorporation of Cs into the unit cell.

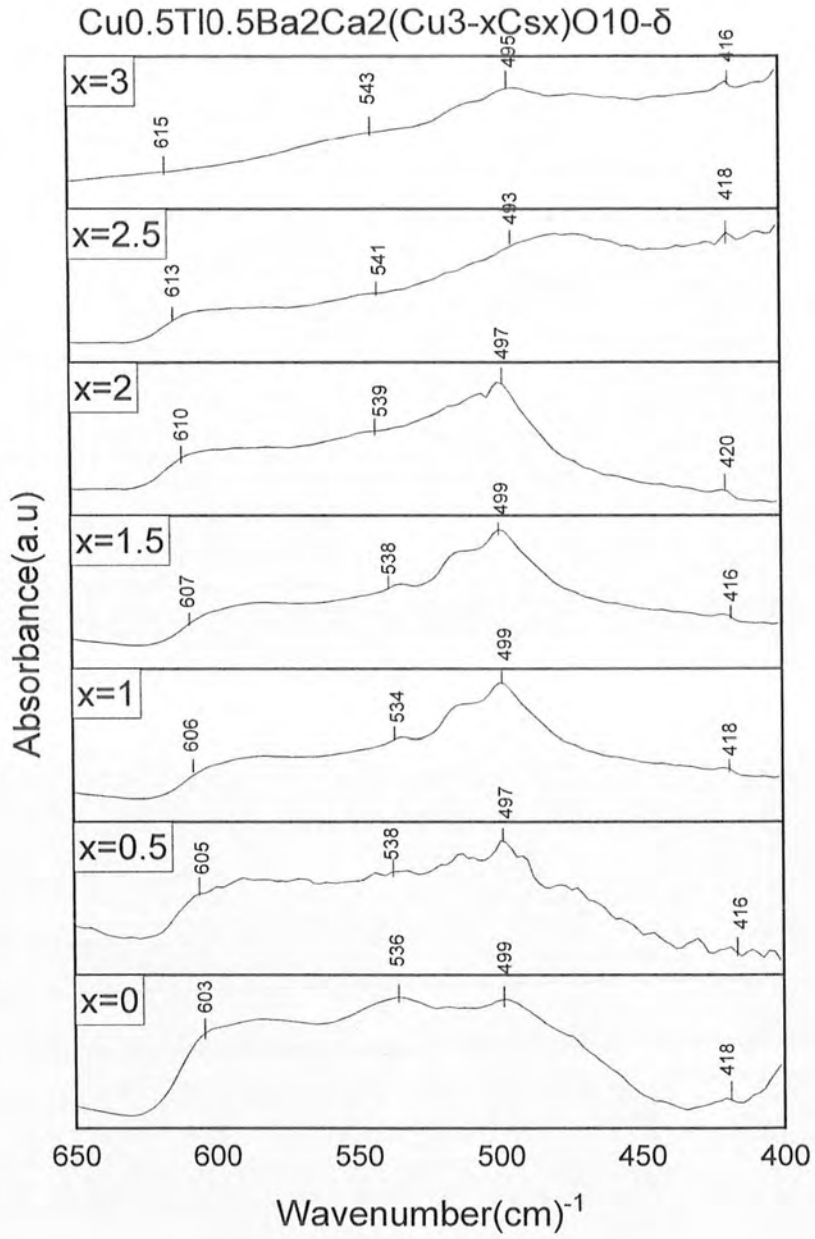

Figure 4-14:FTIR Absorption Spectra of a $Cu_{0.5}Tl_{0.5}Ba_2Ca_2(Cu_{3-x}Cs_x)O_{10-\delta}$ (x=0.5,1,1.5,2,2.5,3) samples

4.3.5 Dielectric Measurement

Dielectric measurements of $Cu_{0.5}Tl_{0.5}Ba_2Ca_2(Cu_{3-x}Cs_x)O_{10-\delta}$(x=0.5,1,1.5,2,2.5,3)samples are shown in Fig4-15, Fig4-16, Fig4-17, and Fig4-18 using the real part of the dielectric constant and the imaginary part of the dielectric constant.

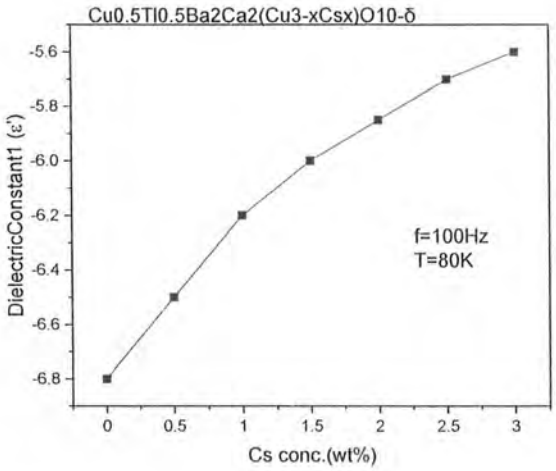

Figure 4-15: Variation of real dielectric constant ε' of a $Cu_{0.5}Tl_{0.5}Ba_2Ca_2(Cu_{3-x}Cs_x)O_{10-\delta}$ with different Cs concentrations beyond Tc at 100Hz

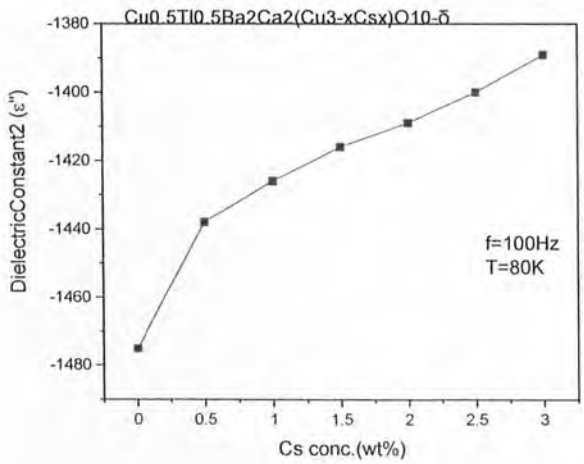

Figure 4-16:Variation of imaginary dielectric constant ε'' of a $Cu_{0.5}Tl_{0.5}Ba_2Ca_2(Cu_{3-x}Cs_x)O_{10-\delta}$ with different Cs concentrations beyond Tc at 100Hz.

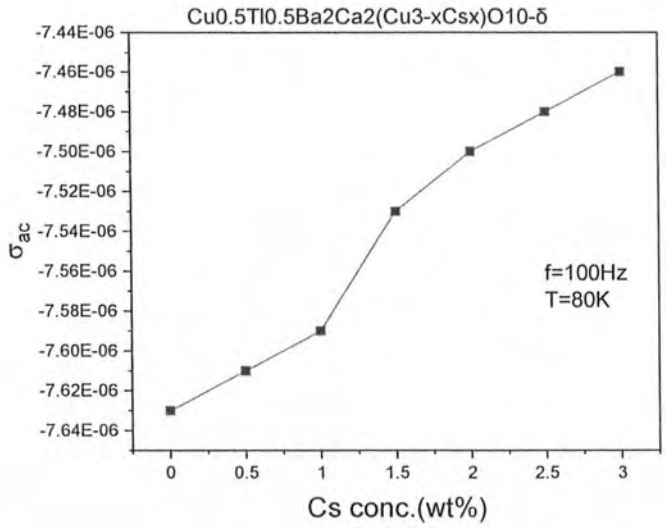

Figure 4-17:Variation of a AC-Conductivity of a $Cu_{0.5}Tl_{0.5}Ba_2Ca_2(Cu_{3-x}Cs_x)O_{10-\delta}$ with different Cs concentrations beyond Tc at 100Hz

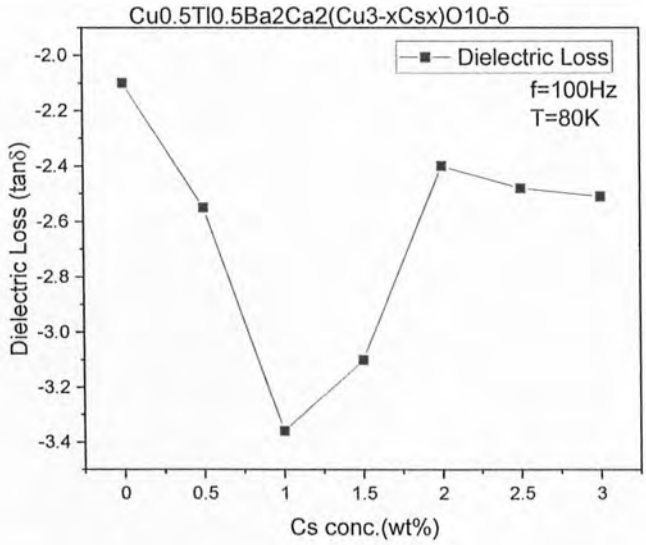

Figure 4-18: Variation of Dielectric loss(tanδ) of a $Cu_{0.5}Tl_{0.5}Ba_2Ca_2(Cu_{3-x}Cs_x)O_{10-\delta}$ with different Cs concentrations beyond Tc at 100Hz

In the final compound,Cs doping suppresses the real part dielectric constant ε',its imaginary part ε'', the dielectric loss and the ac-conductivity; the dielectric loss of suppresses with increased Cs doped samples. The suppression of these parameters' values with increased Cs-doping suggested that the electron donor nature of alkali metal increases the electron concentration in the conducting CuO2/CsO2 planes, suppressing the hole concentration and thus the values of these parameters; holes are majority carriers in the superconducting state.The values of ε', ε'' and σ_{ac} are suppressed in the Cs-doped samples due to the low density in the superconducting state.

4.4 Conclusion

$Cu_{0.5}Tl_{0.5}Ba_2Ca_2(Cu_{3-x}Cs_x)O_{10-\delta}$ (x=0.5,1,1.5,2,2.5,3) superconductor samples are synthesized in order to investigate the role of alkali atoms at CuO_2 planar sites. Alkali atoms are good carriers suppliers, and their presence in the conducting CuO_2 planes may put the material in the under-dope regime of carriers doping in the superconducting state via enhanced electron-hole recombination processes. All of these samples exhibit an orthorhombic structure, with increasing c-axis length but suppressed unit cell volume due to increased Cs doping in the final compounds. So these samples have metallic fluctuations of resistivity in the resistivity measurements from room temperature down to 77K.. These samples show the onset of superconductivity at about 107.9, 106.6, 107.1, 104.5, 109.2, 112.8, 120.8K and show the zero resistivity critical temperature at 91.9, 95.7, 88.9, 94.2, 91.2, 90.3, 95.3K, respectively, in a $Cu_{0.5}Tl_{0.5}Ba_2Ca_2(Cu_{3-x}Cs_x)O_{10-\delta}$ (x=0.5,1,1.5,2,2.5,3) superconductor samples. The excess conductivity analyses of conductivity data of these samples showed improved values of parameters such as $\xi_{c(0)}$,interlayer coupling J and V_F (a Fermi velocity) of superconducting carriers and the phase relaxation time of the superconducting with enhanced in Cs-doped in the final compound. The increase in the values of these parameters is most likely due to arises an increase in the Fermi vector of the carriers $K_F = [3\pi^2N/V]^{1/2}$ which is dependent on the density of carriers which shows enhancement in the density

of carriers in the superconducting CuO_2/CsO_2 planes in Cs-doped samples. The values of these parameters such as the $B_{c(0)}$, $B_{c1(0)}$, $B_{c2(0)}$, $J_c(0)$ and $\kappa=\lambda/\xi$ are are suppressed in Cs-doped $Cu_{0.5}Tl_{0.5}Ba_2Ca_2(Cu_{3-x}Cs_x)O_{10-\delta}$ (x=0.5,1,1.5,2,2.5,3) samples when compared to an un-doped $Cu_{0.5}Tl_{0.5}Ba_2Ca_2Cu_3O_{10-\delta}$ samples showing decrease in the population of inadvetent defects acting as efficient pinning centers. The FTIR absorption measurements revealed all softening of all oxygen-related vibration modes,indicating intric doping in a final compound.At last the dielectric measurements for these samples, the real part of a dielectric constant ε', the imaginary of part of a dielectric constant $i\varepsilon''$ and the ac-conductivity σ_{ac} are here suppressed in Cs-doped $Cu_{0.5}Tl_{0.5}Ba_2Ca_2(Cu_{3-x}Cs_x)O_{10-\delta}$ (x=0.5,1,1.5,2,2.5,3) samples.Suppresion of the values of these parameters by enhanced Cs-doping suggests that the electron donar nature of alkali metals increases the electron concentration on the CuO_2/CsO_2 conducting planes that suppresses the hole concentration through enhanced electron-holes recombination processes.

4.5 References

[1] A.K. Bandyopadhyay, D. Varandani, E. Gmelin, A. V. Narlikar, Phys. Rev. B 50.1 (1994) 462–467

[2] S. Isber, R. Awad, A.I. Abou-Aly, M. Tabbal, J.M. Kaouar, Supercond. Sci. Technol.18.3 (2005) 311–318

[3] A. A. Khurram, A. Ullah, N A. Khan. J. Alloys Compd.481 (2009) 65-69

[4] I. Felner, I. Nowik, E.R. Bauminger, D. Hechel, U. Yaron, Phys. Rev. Lett. (1990) 1945–1951

[5] V.N. Vieira, P. Pureur, J. Schaf, Phys. Rev. B - Condens. Matter Mater. Phys. (2002) 3038–3041

[6] K.A. Jasim, T.J. Alwan, J. Supercond. Nov. Magn. (2017) 3451–3457

[7] A. Raza, S.H. Safeer, N.A. Khan, J. Supercond. Nov. Magn. (2017) 1153-1160.

[8] M. Rahim, N.Khan, J. Alloys Compd, (2009) 81-86.

[9] B. Shabbir, A. Ullah, N. Hassan, M. Irfan, N.A. Khan, in: J. Supercond. Nov. Magn., (2011) 1521-1526.

[10] N.A. Khan, A. Saba, A. Raza, J. Alloys Compd. 757 (2018) 476–483.

[11] N.A. Khan, M. Rahim, M. Mumtaz, Phys. C Supercond. Its Appl. (2012) 3171-3194.

[12] W.E. LawrenceS. Doniach, in:Eizo Kanda (Ed.), Proceedings of the Twelfth International Conference on Low Temperature Physics, Keigaku, Tokyo, 361 (1971)

[13] A.L. Solovjov, H.U. Habermeier, T. Haage, Low Temp. Phys. (2002) 99-108.

[14] A.I. Abou Aly, I.H. Ibrahim, R. Awad, A. El-Harizy, A. Khalaf, J. Supercond. Nov. Magn.